ANNALS OF PHYSICS **148**, 381–435 (1983)

Hypernuclear Spectroscopy in the p Shell*

E. H. AUERBACH, A. J. BALTZ, C. B. DOVER, A. GAL,†
S. H. KAHANA,‡ L. LUDEKING,# AND D. J. MILLENER

Brookhaven National Laboratory, Upton, New York 11973

Received January 10, 1983

A comprehensive shell-model approach to Λ-hypernuclear spectroscopy in the p shell is developed. The available data on the spectra of ${}^{9}_{\Lambda}Be$, ${}^{12}_{\Lambda}C$, ${}^{13}_{\Lambda}C$, ${}^{14}_{\Lambda}N$ and ${}^{16}_{\Lambda}O$ are interpreted in this framework, leading to constraints on the residual ΛN interaction and the one-body Λ-nucleus potential. The mechanism for the formation of Λ hypernuclei via the (K^-, π^-) reaction is treated in the relativistic distorted wave approximation, with careful attention paid to Fermi-averaging of the elementary $K^- n \to \pi^- \Lambda$ amplitude and recoil corrections. Departures from the simple weak coupling picture, arising from configuration mixing, are emphasized. This leads to approximate dynamical symmetries in hypernuclei which are forbidden in ordinary nuclei by the Pauli principle. Further experiments in the p shell are suggested which may reveal other aspects of ΛN interactions.

1. INTRODUCTION

In the past few years, the possibilities for investigating hypernuclear structure have been augmented considerably by the development of magnetic spectrometer systems for the study of the strangeness-changing (K^-, π^-) reaction on nuclear targets. The (K^-, π^-) process has been exploited at CERN [1–5] and Brookhaven [6, 7] to determine the spectrum of ground and excited states for a number of light Λ hypernuclei. The new information on the energies and relative intensities of excited hypernuclear states as seen in the (K^-, π^-) reaction represent a crucial supplement to the ground state binding energies already available for $A \leqslant 16$ from emulsion studies [8].

The new hypernuclear data, particularly those for the p-shell systems ${}^{9}_{\Lambda}Be$, ${}^{12,13}_{\Lambda}C$, ${}^{14}_{\Lambda}N$ and ${}^{16}_{\Lambda}O$, invite a complete treatment in the context of the shell model. The object of this paper is to develop such an approach, with careful attention to the dual problems of reaction mechanism and hypernuclear structure and their interplay. An outline of this program, together with results for ${}^{13}_{\Lambda}C$, is contained in an earlier letter

*The submitted manuscript has been authored under contract DE-AC02-76CH00016 with the U.S. Department of Energy. The U.S. Government's right to retain a nonexclusive royalty-free license in and to the copyright covering this paper, for governmental purposes, is acknowledged.

†Permanent address: The Hebrew University, Jerusalem, Israel; supported in part by the U.S.–Israel Binational Science Foundation.

‡Present address: CEN Saclay, on leave from Brookhaven National Laboratory.

#Present address: North Carolina State University, Raleigh, North Carolina 27650.

0003-4916/83 $7.50

[9]. In the present paper, we provide a more complete picture of the hypernuclear structure and (K^-, π^-) reaction calculations, as well as extending the results of Ref. [9] to encompass other p-shell systems.

The development of this paper proceeds as follows: In Section 2, we discuss our treatment of the reaction mechanism. A distorted wave Born approximation (DWBA) is used, modified to allow for a relativistic description of K^- and π^- propagation. This improves on the standard eikonal approach [10, 11], in that recoil corrections are properly treated. This is particularly important in obtaining the absolute cross sections for *coherent* $n \to \Lambda$ transitions (for instance, $^{12}C(0^+) \to {}^{12}_{\Lambda}C(0^+)$). Elastic K^- and π^- scattering data [12] are fitted to obtain optical potentials and distorted wave functions for the K^- and π^-; the microscopic "$t\rho$" impulse approximation to the optical potential, which is commonly applied, does not yield an adequate fit to the elastic data, and results in different (K^-, π^-) cross sections as well. The DWBA calculations are performed with the relativistic option of the program CHUCK [13], where the K^- and π^- potentials are inserted into an energy-dependent Schrödinger equation derived from a Klein–Gordon equation. Combined with the relativistic treatment of the K^- and π^- distorted waves, we use experimental data and partial wave analyses for the reaction $K^- n \to \pi^- \Lambda$ [14] to obtain a Fermi-averaged transition *amplitude* in the nucleus. For coherent transitions $p_N \to p_\Lambda$, it is important to use the absolute square of a Fermi-averaged amplitude rather than the Fermi average of a cross section in order to obtain the correct absolute size of the (K^-, π^-) cross section to a particular final state.

Combined with the distorted wave approach, one must employ a shell-model formalism sophisticated enough to describe comprehensively the hypernuclear structure aspects. This formalism is developed in Section 3. Care is required, for example, in disentangling the one-body Λ-nucleus spin–orbit potential from the ΛN ressidual interaction, and in analyzing relative production cross sections which differ markedly from the weak-coupling limit. The structure calculation of Ref. [9] included $(0s_N)^4(0p_N)^8(0p_\Lambda)$ and $(0s_N)^4(0p_N)^8(0s_\Lambda)$ configurations in ${}^{13}_{\Lambda}C$; the former lead to the $p_N^{-1}p_\Lambda$ excitations which are predominant in the experimental spectrum of Ref. [7]. A natural treatment of these is central to our approach. Our procedure is to first define a basis of weak-coupling configurations

$$\Psi_{JT_c}({}^{A}_{\Lambda}Z) = [\Psi_{\alpha_c J_c T_c}({}^{A-1}Z) \otimes \Phi_{j_\Lambda}(\Lambda)]^{JT_c}, \tag{1.1}$$

consisting of a Λ coupled to an exact core state $\Psi_{\alpha_c J_c T_c}$. A sufficient number of core states are included and the hypernuclear Hamiltonian

$$H = H_N + H_Y + V_{NY} \tag{1.2}$$

is diagonalized in this truncated weak-coupling basis. For the purely nuclear Hamiltonian H_N given by

$$H_N = \sum_{i=1}^{A-1} h_i + \sum_{i<j} V_{ij} \tag{1.3}$$

we consider two choices for the NN interaction V_{ij}, one due to Cohen and Kurath [15] and the other to Millener [16]. The remaining terms in Eq. (1.2) are the hyperon single-particle Hamiltonian H_Y, defined by a set of single-particle energies, and the hyperon–nucleon residual interaction V_{NY} given by

$$V_{NY} = \sum_{i=1}^{A-1} v(\mathbf{r}_i - \mathbf{r}_Y). \tag{1.4}$$

The form of $v(\mathbf{r}_i - \mathbf{r}_Y)$ includes central components of spin-independent, spin–spin and space-exchange character, and may include as well spin–orbit and tensor components.

Section 4 is devoted to the choice of optical potentials $U(r)$ and bound-state wave functions. The former are taken to have a standard Woods–Saxon form

$$\begin{aligned} U(r) &= -V(r) - iW(r), \\ V(r) &= V_0 \left(1 + \exp\left(\frac{r - R_V}{a_V}\right)\right)^{-1}, \\ W(r) &= W_0 \left(1 + \exp\left(\frac{r - R_W}{a_W}\right)\right)^{-1}, \end{aligned} \tag{1.5}$$

where $R_{V,W} = r_0^{V,W} A^{1/3}$. The parameters are adjusted to obtain a best fit to the elastic $K^- + {}^{12}C$ and $\pi^- + {}^{12}C$ data at 800 MeV/c [12]. The same values of V_0, W_0, $a_{V,W}$ and $r_0^{V,W}$, independently obtained for K^- and π^-, are adopted throughout the p-shell. For neutron bound-state wave functions, we also use a Woods–Saxon potential, adjusting its parameters to fit the neutron binding energy. The parameters were further constrained by fitting binding energies and rms radii for p-shell protons in ${}^{12}C$ and ${}^{13}C$, as obtained from elastic electron scattering and Coulomb energies. The Λ binding energies in p-states are not well known. Experimentally, the $p_{1/2}$ and $p_{3/2}$ Λ orbits have essentially zero binding in ${}^{12}_{\Lambda}C$ [6]. For lighter systems, we have arbitrarily assumed a small binding of order 0.1 MeV for the p-state Λ. The geometry of the Λ well is taken to be the same as that for the neutron.

In Section 5, we present the main body of our results for p-shell hypernuclear structure. We analyse the existing data on ${}^{9}_{\Lambda}Be$, ${}^{12}_{\Lambda}C$, ${}^{13}_{\Lambda}C$, ${}^{14}_{\Lambda}N$ and ${}^{16}_{\Lambda}O$, and discuss the prospects for extracting additional information from the as yet unexplored systems ${}^{10}_{\Lambda}B$, ${}^{11}_{\Lambda}B$, ${}^{14}_{\Lambda}C$ and ${}^{15}_{\Lambda}N$. The emphasis of this work is on the extraction, from the hypernuclear spectrum, of details of the ΛN interaction not otherwise obtainable directly from experiment. We would also like to isolate those features of the spectra which result uniquely from the presence of the distinguishable Λ particle in the nucleus. The existence of hypernuclear states with a high degree of spatial symmetry, not allowed in ordinary nuclei, leads to approximate dynamical selection rules in the (K^-, π^-) process. We also pinpoint hypernuclear γ transitions due to "pure" Λ single-particle transitions, which lead to an accurate determination of Λ spin-orbit

splittings. Some of these may be observable experimentally via the $(K^-, \pi^-\gamma)$ reaction [17].

A brief summary of our conclusions is given in Section 6.

2. The (K^-, π^-) Reaction Mechanism

A proper relativistic calculation of the mechanism for the reaction ${}^{A}Z(K^-, \pi^-){}^{A}_{\Lambda}Z$ is not easily accomplished even within a distorted-wave framework. We shall short-circuit this treatment to some extent by providing an ansatz for the many-body reaction amplitude in the rest frame of the target nucleus, i.e., in the laboratory system. This amplitude is assumed to be given additively in terms of the interaction of the K^- meson with each nucleon in the target. Hence one requires in principle a knowledge of the amplitude for the elementary $K^-n \to \pi^-\Lambda$ process in a variety of off-shell situations. Rather than treating this off-shell behavior we employ an amplitude possessing explicit Lorentz invariance and energy-averaged over the bound nucleon energies. We extrapolate from the elementary amplitude to the many-body amplitude with an explicit model form for the $K^-n \to \pi^-\Lambda$ interaction.

2.1. *Construction of the* (K^-, π^-) *Distorted-Wave Amplitude*

The cross section for hypernuclear production in the (K^-, π^-) reaction depicted in Fig. 1a may be written in the laboratory frame as [18]

$$\frac{d\sigma}{d\Omega_L} = J \frac{(k_\pi/k_K)}{(2\pi\hbar^2c^2)^2} \frac{\Pi E}{(E_{\text{total}})^2} \overline{|T^B_{if}|^2} \tag{2.1}$$

with ΠE defined as the product of the energies of the K^-, π^-, target (A) and residual hypernucleus (H) in the barycentric system, and k_π, k_K are the many-body barycentric momenta. The total c.m. energy is $E_{\text{total}} = E_\pi + E_H = E_K + E_A$, and J is the barycentric to lab Jacobian. The bar denotes the appropriate average and summation over spins. The transition amplitude T^B_{if} is defined here in the many-body barycentric system, including distortion, as

$$\begin{aligned} T^B_{if} = \int \chi^{(-)*}(\mathbf{k}_\pi, \mathbf{r}_{\pi H}) \langle {}^{A}_{\Lambda}Z(f) | (\mathbf{r}_\pi, \mathbf{r}_\Lambda | v | \mathbf{r}_K, \mathbf{r}_n) \Phi^\dagger_\Lambda(\mathbf{r}_{\Lambda c}) \Phi_n(\mathbf{r}_{nc}) | {}^{A}Z(i) \rangle \\ \times \chi^{(+)}(\mathbf{k}_K, \mathbf{r}_{KA})\, d^3r_{\pi H} d^3r_{\Lambda c} d^3r_{KA} d^3r_{nc} \end{aligned} \tag{2.2}$$

with coordinates as given in Fig. 1b. Here $\Phi_n(\mathbf{x})|\Phi^\dagger_\Lambda(\mathbf{y})|$ is the second-quantized field operator destroying (creating) a neutron (Λ) at the spatial point $\mathbf{x}(\mathbf{y})$:

$$\Phi_n(\mathbf{x}) = \sum_{j_n, m_n} \phi_{j_n m_n}(\mathbf{x})\, a_n(j_n, m_n), \tag{2.3a}$$

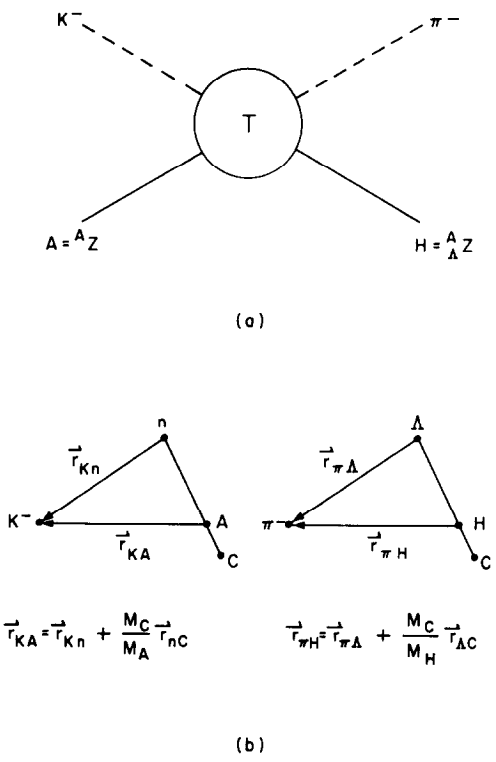

FIG. 1. Notation for the discussion of the (K^-, π^-) reaction on a nuclear target A, leading to a hypernucleus H. In the initial and final channels $K^- + A$ and $\pi^- + H$, respectively, the vector relation between the two-body and many-body relative coordinates is shown; C is the nuclear core consisting of the $A - 1$ spectator nucleons.

$$\Phi_\Lambda^\dagger(\mathbf{y}) = \sum_{j_\Lambda, m_\Lambda} \phi^*_{j_\Lambda m_\Lambda}(\mathbf{y})\, a_\Lambda^\dagger(j_\Lambda, m_\Lambda). \tag{2.3b}$$

The effective meson–baryon interaction v for the transition $K^- n \to \pi^- \Lambda$ is assumed local and spin-independent,

$$(\mathbf{r}_\pi, \mathbf{r}_\Lambda \,|\, v \,|\, \mathbf{r}_K, \mathbf{r}_n) = \delta(\mathbf{R}_{\pi\Lambda} - \mathbf{R}_{Kn})\, \delta(\mathbf{r}_{\pi\Lambda} - \mathbf{r}_{Kn})\, V(\mathbf{r}_{Kn}), \tag{2.4a}$$

where $\mathbf{R}_{ab}$ denotes the center of mass coordinate constructed from $\mathbf{r}_a$ and $\mathbf{r}_b$. Introducing a multipole expansion for $a_\Lambda^\dagger a_n$, and isospin notation, Eq. (2.2) reduces to the form[1]:

[1] Here and throughout this paper we follow the angular momentum conventions set in Ref. [19]; note, in particular, the definition of reduced matrix elements.

$$T^B_{if} = (T_i \tau_i \, 1/2 \, 1/2 \,|\, T_f \tau_f) \sum_k (J_i M_i k m | J_f M_f) \sum_{j_\Lambda j_N} \beta^k_m(j_\Lambda, j_N) \times \langle f \| (a^\dagger_\Lambda(j_\Lambda) \tilde{a}_N(j_N))^{k1/2} \| i \rangle \tag{2.5}$$

with the distorted-wave reduced amplitude β^k_m given by

$$\beta^k_m(j_\Lambda, j_N) = (-1)^{k+m} \int \chi^{(-)*}(\mathbf{k}_\pi, \mathbf{r}_{\pi H}) (\bar{\phi}_{j_\Lambda}(\mathbf{r}_{\Lambda c}) v \phi_{j_N}(\mathbf{r}_{nc}))^k_{-m} \chi^{(+)}(\mathbf{k}_K, \mathbf{r}_{KA}) \times d^3 r_{\pi H} d^3 r_{\Lambda c} d^3 r_{KA} d^3 r_{nc}. \tag{2.6}$$

The time-reversed quantities denoted by tilde are defined through

$$\tilde{a}_N(j_N, m_N) = (-1)^{j_N + m_N} a(j_N, -m_N), \tag{2.7a}$$

$$\bar{\phi}_{j_\Lambda, m_\Lambda} = (-1)^{j_\Lambda - m_\Lambda} \phi^*_{j_\Lambda, -m_\Lambda}. \tag{2.7b}$$

The reduced (in spin and isospin) matrix elements

$$\langle f \| (a^\dagger_\Lambda \tilde{a}_N)^{k1/2} \| i \rangle \tag{2.8}$$

constitute the one-baryon density matrix appropriate to (K^-, π^-) in terms of the neutron pickup amplitudes from the ${}^A Z$ target, obtained in the structure calculation described below. Averaging the squared amplitude (2.5) over initial, and summing over final, nuclear spin orientations:

$$\overline{|T^B_{if}|^2} \equiv \frac{1}{2J_i + 1} \sum_{M_i M_f} |T^B_{if}|^2 = (T_i \tau_i \, 1/2 \, 1/2 | T_f \tau_f)^2 \frac{(2J_f + 1)}{(2J_i + 1)} \times \sum_{km} \frac{1}{2k+1} \left| \sum_{j_\Lambda j_N} \beta^k_m(j_\Lambda, j_N) \langle f \| (a^\dagger_\Lambda(j_\Lambda) \tilde{a}_N(j_N))^{k1/2} \| i \rangle \right|^2. \tag{2.9}$$

A considerable simplification occurs in the amplitude β^k_m under the assumption that the meson–baryon interaction (2.4a) is of zero range:

$$V(\mathbf{r}_{Kn}) = V^B_I \delta(\mathbf{r}_{Kn}). \tag{2.4b}$$

The δ functions that enforce $\mathbf{r}_{\pi\Lambda} = \mathbf{r}_{Kn} = 0$ in (2.4) give rise to two corollaries: (i) causing $\delta(\mathbf{R}_{\pi\Lambda} - \mathbf{R}_{Kn})$ to become equivalent to

$$\delta(\mathbf{r}_{\Lambda c} - \mathbf{r}_{nc}) \tag{2.10a}$$

and, through the relationships noted in the caption to Fig. 1, (ii) $\delta(\mathbf{r}_{\pi\Lambda} - \mathbf{r}_{Kn}) \delta(\mathbf{r}_{Kn})$ may be replaced by

$$\delta\left(\frac{M_c}{M_A} \mathbf{r}_{nc} - \mathbf{r}_{KA}\right) \delta\left(\mathbf{r}_{\pi H} - \frac{M_A}{M_H} \mathbf{r}_{KA}\right). \tag{2.10b}$$

With the constraints given by (2.10), expression (2.6) simplifies:

$$\beta_m^k(j_\Lambda, j_N) = \left(\frac{M_A}{M_c}\right)^3 V_I^B \int d^3 r \chi^{(-)*}\left(\mathbf{k}_\pi, \frac{M_A}{M_H}\mathbf{r}\right)(-)^{k+m}\left(\bar{\phi}_{j_\Lambda}\left(\frac{M_A}{M_c}\mathbf{r}\right)\right.$$
$$\left.\times \phi_{j_N}\left(\frac{M_A}{M_c}\mathbf{r}\right)\right)_{-m}^{k} \chi^{(+)}(\mathbf{k}_K, \mathbf{r}). \tag{2.11}$$

The factor $(M_A/M_c)^3$ must be externally factored into the CHUCK calculations.

Since we have ignored spin flip in the $K^- n \to \pi^- \Lambda$ process, we can decouple spin in (2.11) in order to identify the angular momentum transfer ΔJ as $\Delta J = \Delta L = k$:

$$\beta_m^k(j_\Lambda, j_N) = \left[\frac{(2j_N+1)(2l_\Lambda+1)}{4\pi(2k+1)}\right]^{1/2}(-)^{l_N}(l_\Lambda 0 l_N 0|k0)\, U\left(l_\Lambda \frac{1}{2} k j_N, j_\Lambda l_N\right)$$
$$\times \left\{\left(\frac{M_A}{M_c}\right) V_I^B \int_0^\infty dr u_{j_\Lambda l_\Lambda}\left(\frac{M_A}{M_c} r\right) u_{j_N l_N}\left(\frac{M_A}{M_c} r\right)\right.$$
$$\left.\times \int \left(d\Omega \chi^{(-)*}\left(\mathbf{k}_\pi, \frac{M_A}{M_H}\mathbf{r}\right) Y_m^{k*}(r)\, \chi^{(+)}(\mathbf{k}_K, \mathbf{r})\right)\right\}. \tag{2.12}$$

The factor $(l_\Lambda 0 l_N 0|k0)$ exhibits the natural parity selection rule $l_\Lambda + l_N + k = \text{even}$.

2.2. *Comparison to Eikonal Calculations*

We note particularly in Eq. (2.11) the coordinates $\mathbf{r}$ and $M_A\mathbf{r}/M_H$ which appear in the outgoing and incoming distorted waves, respectively. In the context of the three-body model of Fig. 1, these coordinates take proper account of recoil corrections and include effects of the Λ-neutron mass difference. The fact that $\bar{\phi}_{j_\Lambda}(\mathbf{r})$ and $\phi_{j_N}(\mathbf{r})$ are evaluated at the same spatial coordinate is a consequence of the zero-range approximation we have used for the $K^- n \to \pi^- \Lambda$ amplitude. In Ref. [20], the (K^-, π^-) cross sections for a ^{12}C target were evaluated using a momentum-space code which incorporates finite range effects by using the full partial-wave structure of the $K^- n \to \pi^- \Lambda$ process, rather than an effective s-wave approximation as employed here. By comparing the results of coordinate space distorted-wave runs with the earlier calculations [20], we conclude that the finite range of the elementary amplitude has little influence on small-angle cross sections for hypernuclear formation. Note, however, that in the standard eikonal distorted wave approach [10, 11], one neglects recoil corrections, i.e., M_A/M_H and M_A/M_C are set equal to unity in Eq. (2.11). Since $M_A/M_C = A/(A-1) \approx 1 + 1/A$, this would appear to be a harmless neglect of a "$1/A$" correction. We have checked the validity of this procedure for a variety of (K^-, π^-) transitions to discrete final states. For transitions with orbital angular momentum transfer $k = \Delta L \neq 0$ to states in $^{12}_{\Lambda}C$, we have generally found good agreement (on the level of 10–20% or so) between the no-recoil eikonal approximation and the full distorted-wave calculation. However, for $0^+ \to 0^+$ transitions

with $k = 0$, we have found large discrepancies (as much as a factor of 2) between the standard eikonal and distorted-wave (CHUCK) results, even at 0°. Thus, for these transitions, which are the most important for small-angle (K^-, π^-) reactions, it is important to take account of recoil effects, which are much larger than the naive estimate of $1/A$.

As a parallel test, the eikonal program of Ludeking [21], which was used to estimate hypernuclear formation cross sections in the (π^+, K^+) reaction, was modified to include recoil effects in the approximation $M_H \approx M_A$. Note, however, that the correct value of M_H is used to calculate k_π. Expression (2.11) can then be written as

$$\beta_m^k(j_\Lambda, j_N) = V_I^B \int d^3r \chi^{(-)*}(\mathbf{k}_\pi, \mathbf{r})(-)^{k+m}(\bar{\psi}_{j_\Lambda}(\mathbf{r})\, \psi_{j_N}(\mathbf{r}))^k_{-m} \chi^{(+)}(\mathbf{k}_K, \mathbf{r}), \quad (2.13a)$$

$$\psi_j(\mathbf{r}) = \left(\frac{A}{A-1}\right)^{3/2} \phi_j(\boldsymbol{\rho}), \qquad \boldsymbol{\rho} = A\mathbf{r}/(A-1). \quad (2.13b)$$

Provided the normalized wave functions $\phi_j(\boldsymbol{\rho})$ solve the Schrödinger equation with Woods–Saxon potentials of well depth V_0 and geometrical parameters r_0, a to yield binding energy E_B, the wave functions ψ_j are also normalized, $\int |\psi_j|^2 d^3r = 1$, and can be obtained by solving the Schrödinger equation with scaled parameters

$$\{r_0, a\} \to (A-1)/A\{r_0, a\}, \qquad \{V_0, E_B\} \to [A/(A-1)]^2\{V_0, E_B\}.$$

For $k \neq 0$, the eikonal and DWBA results for a test case ${}^{16}O(K^-, \pi^+)^{16}_{\Sigma}C$ at 720 MeV/c were identical within a few percent for $\theta_L \approx 0°$. For $p \to p$, $k = 0$ transitions leading to 0^+ final states in ${}^{16}_{\Sigma}C$, there was still a discrepancy in cross section of about 30%. The discrepancy relevant to Λ hypernuclear production in (K^-, π^-) is estimated to be smaller for $k = 0$ due to the smaller momentum transfer here and the smaller mass difference $M_H - M_A$. This indicates that the eikonal approximation itself is rather good at 700–800 MeV/c, if one takes account of recoil effects. The modified eikonal program [21] was useful in any case for providing an independent check of the normalizations, angular momentum and isospin phases, and the integration procedures of the DWBA calculation.

In the plane-wave limit the curly bracket of (2.12) simplifies ($M_H \simeq M_A$) to

$$\begin{aligned} \{\ \} &\to V_I^B \int d\Omega\, dr\, e^{i\mathbf{q}'\cdot\mathbf{r}}\, Y_m^{k*}(\hat{r})\, u_{j_\Lambda l_\Lambda}(r)\, u_{j_N l_N}(r) \\ &= V_I^B\, 4\pi i^k Y_m^{k*}(\hat{q}) \int_0^\infty dr\, u_{j_\Lambda l_\Lambda}(r) j_k(q'r)\, u_{j_N l_N}(r), \end{aligned} \quad (2.14)$$

where $\mathbf{q}' = (M_c/M_A)\,\mathbf{q}$ and $\mathbf{q} = \mathbf{k}_K - \mathbf{k}_\pi$ is the c.m. momentum transfer. For small values of q, the factor $j_k(q'r) \sim (q'r)^k$ produces a characteristic peaking which for $k \neq 0$ occurs at a nonzero angle which increases with k. This feature remains evident in the distorted-wave amplitudes and can be seen in the angular distributions plotted in Section 5.

2.3. *Computational Procedure and Choice of V_I*

In practice [22], the partial-wave expansion

$$\chi^{(+)}(\mathbf{k}_K, \mathbf{r}) = \frac{4\pi}{k_K r} \sum_{l_i m_i} i^{l_i} u_{l_i}(k_K, r)\, Y^{l_i *}_{m_i}(\hat{k}_K)\, Y^{l_i}_{m_i}(\hat{r}),$$
$$\chi^{(-)*}(\mathbf{k}_\pi, \mathbf{r}) = \frac{4\pi}{k_\pi r} \sum_{l_f m_f} i^{-l_f} u_{l_f}(k_\pi, r)\, Y^{l_f}_{m_f}(\hat{k}_\pi)\, Y^{l_f}_{m_f}(\hat{r}) \tag{2.15}$$

is introduced into expression (2.12) for β^k_m which then involves the evaluation of one-dimensional integrals containing the radial wave functions $u_{j_\Lambda l_\Lambda}$ and $u_{j_N l_N}$ for the baryons and the partial waves u_{l_i} and u_{l_f} for the mesons. These partial waves $u_l(r)$ are calculated using a Klein–Gordon (KG) equation, which in CHUCK [13] and the program A-THREE [23] used for the elastic fits, is reduced to an energy-dependent Schrödinger equation of the form

$$\left\{\nabla^2 + \frac{1}{\hbar^2}\left[(E^2/c^2 - m^2c^2) - 2E(U + V_c)/c^2\right]\right\} \chi = 0. \tag{2.16}$$

From the imaginary part of the optical potential one can compute a mean free path λ_M for the K^- and π^- inside nuclei. Anticipating depths of $W_0 \approx 50$MeV from Section 4, one finds that λ_M is of the order of the nuclear radius for the p-shell nuclei. Thus the potentials are not very strongly absorbing at these rather high projectile energies.

Finally, we discuss the choice of the volume integral V_I^B (2.4b) in the barycentric frame. A straightforward application of the zero-range assumption (2.10) without recourse to the previous expansions, yields for T^B_{if}, Eq. (2.2), the following expression ($M_H \approx M_A$ assumed):

$$T^B_{if} = V_I^B \int \chi^{(-)*}(\mathbf{k}_\pi, \mathbf{r})\, \rho^{\Delta S=-1, \Delta Q=0}_{if}(\mathbf{r})\, \chi^{(+)}(\mathbf{k}_K, \mathbf{r})\, d^3r. \tag{2.17a}$$

Here, the strangeness-changing charge-conserving transition density

$$\rho^{\Delta S=-1, \Delta Q=0}_{if}(\mathbf{r}) = \left\langle f \left| \sum_{\alpha,\beta} \psi^*_\beta(\mathbf{r})\, \psi_\alpha(\mathbf{r})\, a^+_\Lambda(\beta)\, a_n(\alpha) \right| i \right\rangle, \tag{2.17b}$$

where the scaled and dilated single-particle wave functions are defined by (2.13b), may also be written in the more familiar form

$$\rho^{\Delta S=-1, \Delta Q=0}_{if}(\mathbf{r}) = \int \Psi^*_f(\{\mathbf{r}_j, \boldsymbol{\sigma}_j, \mathbf{u}_j\}) \left(\sum_1^A u^-(j)\, \delta(\mathbf{r} - \mathbf{r}_j)\right) \Psi_i(\{\mathbf{r}_j, \boldsymbol{\sigma}_j, \mathbf{u}_j\})\, \Pi d^3 r_j \tag{2.17c}$$

with $u^-(j)$ the lowering component of u spin required to transform a neutron j to a Λ

in the same space-spin state. The coordinate $\mathbf{r}_j$ is relative to the nuclear center of mass, so that (2.17b, c) provide the required generalization of static charge densities (elastic as well as inelastic) as measured by electron scattering. The form (2.17a) is reminiscent of the "$t\rho$" approximation for inelastic processes at medium energies, where t is the two-body transition amplitude. However, the most natural frame to impose this approximation is the laboratory frame, in which the prescription $T^L = t^L(0°)\rho$, embodying in addition a zero-range assumption for the two-body effective interaction, gives rise to

$$T^L_{if} = t^L(0°) \int \chi^{(-)*}(\mathbf{k}_\pi, \mathbf{r})\, \rho^{\Delta S=-1, \Delta Q=0}_{if}(\mathbf{r})\, \chi^{(+)}(\mathbf{k}_K, \mathbf{r})\, d^3r. \tag{2.18}$$

Since, by Lorentz invariance [18],

$$\sqrt{(E_K E_\Lambda E_\pi E_H)_L}\; T^L = \sqrt{(E_K E_\Lambda E_\pi E_H)}\; T^B, \tag{2.19}$$

expressions (2.17a) and (2.18), upon comparison, yield the identification

$$V^B_I = \sqrt{\frac{\Pi E_L}{\Pi E}}\, V_I, \qquad V_I = |t^L(0°)|. \tag{2.20a}$$

An explicit expression for the volume integral V_I is given by

$$V_I = 2\pi(\hbar c)^2 \left[\frac{p_{K^-}}{p_{\pi^-}\varepsilon_K \varepsilon_\pi}\left(1 - \frac{q\varepsilon_{\pi^-}}{\varepsilon_\Lambda p_{\pi^-}}\right)\frac{d\sigma(K^- n \to \pi^- \Lambda)}{d\Omega_L(0°)}\right]^{1/2}, \tag{2.20b}$$

where the small case quantities refer to the two-body lab system. Expressions (2.1), (2.17a) and (2.20a) for the (K^-, π^-) laboratory cross section are equivalent to Eqs. (2) of our letter [9].

The assumption of zero meson–baryon interaction range is here equivalent to $t \approx t(0°)$ which is justified even for the largest angles observed in present (K^-, π^-) experiments where the momentum transfer is less than 300 MeV/c, much smaller than the momentum $1/\Delta r \approx 500$–1000 MeV/c associated with the range Δr of the $K^- n \to \pi^- \Lambda$ interaction.

2.4. *Fermi Averaging*

Another point in selecting the appropriate strength for the $K^- n \to \pi^- \Lambda$ amplitude in the nuclear medium is the strong energy dependence of the free-space amplitude in the momentum region around 800 MeV/c where most data exist. In view of this, it is important to average the amplitude over the distribution of neutron momenta in the nucleus. We now define our procedure for this Fermi averaging.

Several groups [24, 25] have presented multichannel analyses of the $\bar{K}N \to \bar{K}N$, $\pi\Lambda$ and $\pi\Sigma$ amplitudes. For computing the appropriate Fermi-averaged amplitudes for the $K^- n \to \pi^- \Lambda$ reaction on nuclear targets, we have adopted the amplitudes due to Gopal *et al.* [24], which are available in the total center of mass energy range

1480–2170 MeV. Although the free-space amplitudes of Martin and Pidcock [25] exhibit some significant differences from those of Gopal *et al.* [24] for certain partial waves, the Fermi-averaged results are very similar, since one sums over partial waves and smooths out rapid energy dependences by the averaging procedure.

In the two-body barycentric system, one has the usual partial-wave decomposition of the non-spin-flip and spin-flip amplitudes f_B and g_B

$$\begin{aligned} f_B(\theta) &= \frac{1}{\kappa}\sum_l [(l+1)\,T_{l+} + lT_{l-}]\,P_l(\cos\theta), \\ g_B(\theta) &= \frac{1}{\kappa}\sum_l [T_{l+} - T_{l-}]\,P_l^1(\cos\theta) \end{aligned} \tag{2.21}$$

such that

$$\left(\frac{d\sigma}{d\Omega}\right)_B^{K^-n\to\pi^-\Lambda} = |f_B(\theta)|^2 + |g_B(\theta)|^2. \tag{2.22}$$

Here κ is the K^-n barycentric momentum, and the dimensionless amplitudes $T_{l\pm}$ refer to the total spin $j = l \pm \frac{1}{2}$, respectively.

For $\theta = 0°$, the relation between barycentric and lab cross sections assumes the simple form

$$\left(\frac{d\sigma}{d\Omega_L}\right)_{0°}^{K^-n\to\pi^-\Lambda} \equiv |f_L(0)|^2 = \left(\frac{k_{\pi L}}{k_\pi}\right)^2 \left(\frac{d\sigma}{d\Omega}\right)_{B,0°}^{K^-n\to\pi^-\Lambda}, \tag{2.23}$$

where $k_{\pi L}$ and $k_\pi = \kappa'$ are the momentum of the pion in the final-state two-body lab and barycentric systems, respectively.

Our Fermi-averaging procedure is done in the lab system, for $\theta = 0°$. Equivalently, if one writes the amplitude as a function of the relativistic variables s and t, we are essentially keeping t fixed and averaging over s. No off-shell corrections are included, such as binding energy, Pauli principle and dispersive effects of the nuclear medium. In our calculation, the only effect of the nucleus is to generate a distribution $\rho(k)$ of the lab momentum $\mathbf{k}$ of the struck neutron in the $K^-n \to \pi^-\Lambda$ reaction. If we define the z axis as the direction of the incident lab momentum p_K of the K^-, our Fermi average consists in integrating over the magnitude of $\mathbf{k}$ and also $x = \cos\theta_{p_K,\mathbf{k}}$. We define two types of averages

$$\begin{aligned} \left\langle \frac{d\sigma}{d\Omega_L} \right\rangle_{0°,\mathrm{AV}} &= \int_0^\infty dk\, k^2 \rho(k) \int_{-1}^{+1} dx \left(\frac{d\sigma}{d\Omega_L}\right)_{0°} (p_K, k, x), \\ \langle f_L(0)\rangle_{\mathrm{AV}} &= \int_0^\infty dk\, k^2 \rho(k) \int_{-1}^{+1} dx f_L(0), \end{aligned} \tag{2.24}$$

where $\rho(k)$ is normalized so that $2\int_0^\infty dk\, k^2\rho(k) = 1$. The incoherent average $\langle d\sigma/d\Omega_L\rangle_{0°,\mathrm{AV}}$ is appropriate for sum-rule estimates of the total (K^-, π^-) cross

section on a nucleus, summed over final hypernuclear states (including the continuum). For coherent transitions (for instance, $p_N \to p_\Lambda$) of interest in this paper, it is more correct to first average the forward amplitude, obtaining $\langle f_L(0)\rangle_{\rm AV}$, and then square to obtain a cross section, rather than directly averaging the cross section. The difference between $\langle d\sigma/d\Omega_L\rangle_{0^\circ,\rm AV}$ and $|\langle f_L(0)\rangle_{\rm AV}|^2$ is quite significant in the region of interest around 800 MeV/c, as we see later. In $\langle f_L(0)\rangle_{\rm AV}$, $\rho(k)$ should represent only the momentum distribution for the particular single-particle orbit we are considering (p_N here). In the p shell, only a small error is introduced, however, if we instead use the momentum distribution of the entire nucleus for $\rho(k)$.

In detail, the calculation proceeds as follows. We first perform the sum in Eq. (2.21) at each energy to obtain $f_B(0)$, using the $T_{l\pm}$ from Gopal *et al.* (s, p, d, f and g waves are included). We then obtain the lab amplitudes $f_L(0) = (k_{\pi L}/k_\pi) f_B(0)$, using free space two-body kinematics to compute $k_{\pi L}$ and k_π. Using the values of $f_L(0)$ at successive overlapping sets of three values of barycentric energy $\varepsilon_{\rm total}$, we construct a quadratic interpolation formula for $f_L(0)$ in each region of energy. In numerically performing the integrations in Eq. (2.24), we first construct $\varepsilon_{\rm total}$ for each choice of p_K, k and x via the formula

$$\varepsilon_{\rm total} = (m_K^2 + \kappa^2)^{1/2} + (m_N^2 + \kappa^2)^{1/2}, \tag{2.25}$$

$$\kappa^2 = (p_K^2 k^2 x^2 - 2\varepsilon_{p_K}\varepsilon_k p_K k x + p_K^2 M_N^2 + \varepsilon_{p_K}^2 k^2)/(M_K^2 + M_N^2 + 2\varepsilon_{p_K}\varepsilon_k - 2p_K k x),$$

where $\varepsilon_{p_K} = (M_K^2 + p_K^2)^{1/2}$, $\varepsilon_k = (M_N^2 + k^2)^{1/2}$, M_K and M_N being the kaon and nucleon masses, respectively. We then use the interpolation formula to calculate the corresponding value of $(d\sigma/d\Omega_L)_{0^\circ}$ or $f_L(0)$. Thirty grid points in x and a 5 MeV/c grid in k were sufficient for an accurate numerical evaluation.

Results are shown in Figs. 2 to 4. The angular distributions for the free space $K^- n \to \pi^- \Lambda$ reaction at several momenta are shown in Fig. 2. Note that the cross sections do not drop drastically in the angular region between 0 and 15°. Thus the approximation of replacing the full partial wave content of the $K^- n \to \pi^- \Lambda$ process by a Fermi-averaged total amplitude at 0° is quite reasonable for small angle (K^-, π^-) reactions on nuclei. Recall that in our calculation of hypernuclear formation cross sections, we use a zero-range transition operator proportional to $\langle f_L(0)\rangle_{\rm AV} \sum_{i\in n} u^-(i)\,\delta(\mathbf{r} - \mathbf{r}_i)$, i.e., an effective s-wave (isotropic) amplitude. The spin-flip cross section $|g|^2$ is also seen to be very small at 800 MeV/c.

We have performed Fermi-averaging with several different assumptions for $\rho(k)$. One form used is

$$\rho(k) = \rho_0(1 + \exp(k - k_0)/\Delta k)^{-1} \tag{2.26}$$

with $k_0 = 100$ MeV/c and $\Delta k = 50$ MeV/c. This diffuse Fermi gas model was first obtained by Miller [26] and later used by Allardyce *et al.* [27] for the Fermi-

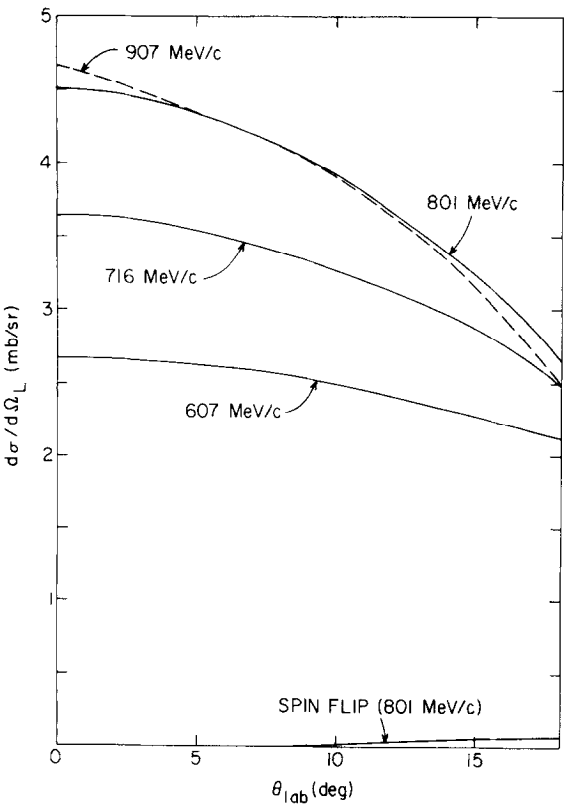

FIG. 2. Differential cross sections for the $K^- n \to \pi^- \Lambda$ reaction in the lab system at several incident momenta, taken from the analysis of Gopal *et al.* [14]. The spin flip cross section is shown separately at 801 MeV/c.

averaging of pion–nucleon amplitudes. For ^{12}C, we have also used a harmonic oscillator model

$$\rho(k) = \rho_0(N_s + 2/3\, N_p(kb)^2)\, e^{-(kb)^2} \tag{2.27}$$

with oscillator length parameter $b = 1.64$ fm. Here N_s and N_p are the number of s- and p-shell neutrons. In Fig. 3, we show results obtained using Eq. (2.26) and also the oscillator model with both $L_N = 0$ and 1 ($N_s = 2$, $N_p = 4$) and with $L_N = 1$ only ($N_s = 0$), the latter being more appropriate to the coherent $p_N \to p_\Lambda$ transitions. The differences are seen to be only a few percent. This may be expected, since the rms momentum $\langle k^2 \rangle^{1/2}$ for the various $\rho(k)$ models is very similar: we have $\langle k^2 \rangle^{1/2} = 177$ and 201 MeV/c for the $L_N = 0, 1$ oscillator and Fermi forms, respectively.

In Fig. 4, we display our results for the coherent and incoherent Fermi-averaged $K^- n \to \pi^- \Lambda$ cross sections, as a function of K^- lab momentum, using $\rho(k)$ from Eq. (2.26). The rapid energy dependence in the free cross section, due to a number of

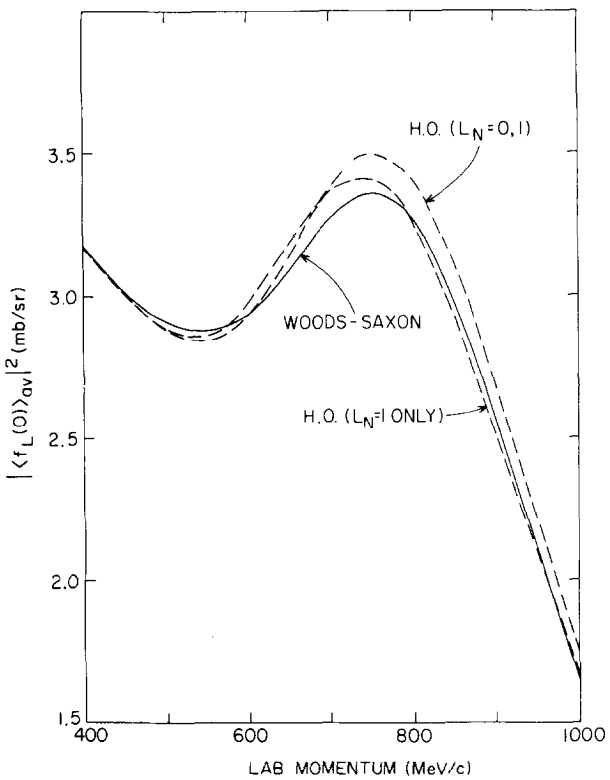

FIG. 3. The absolute square of the Fermi-averaged $K^- n \to \pi^- \Lambda$ lab amplitude $f_L(0)$ as a function of momentum. Several prescriptions for the density $\rho(k)$ used in the Fermi average are compared. The solid curve uses the Woods–Saxon $\rho(k)$ of Eq. (2.26), while the dashed curves use the harmonic oscillator density of Eq. (2.27), including both s- and p-wave nucleons ($L_N = 0, 1$) or only p-shell nucleons (curve labeled "$L_N = 1$ ONLY").

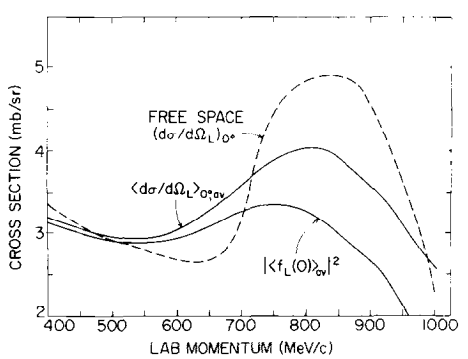

FIG. 4. Fermi-averaged forward $K^- n \to \pi^- \Lambda$ lab cross sections as a function of K^- lab momentum. The free space lab cross section of Gopal *et al.* [14] is displayed as a dashed line. The coherent and incoherent Fermi averages $|\langle f_L(0)\rangle|^2$ and $\langle d\sigma/d\Omega_L\rangle_{0°,av}$ of Eq. (2.24) are shown as solid lines.

Y_1^* resonances, is considerably smoothed out by the averaging procedure. The coherent average $|\langle f_L(0)\rangle_{AV}|^2$ is consistently smaller than the averaged cross section $\langle d\sigma/d\Omega_L\rangle_{0°,AV}$, although the differences are minor below 700 MeV/c or so. At 800 MeV/c, the momentum appropriate to the ${}^{13}_{\Lambda}C$ experiment, $|\langle f_L(0)\rangle_{AV}|^2$ is considerably reduced with respect to the free cross section, by almost a factor of 2. We see that it is also important to include Fermi averaging in sum-rule estimates of (K^-, π^-) cross sections on nuclei. Using $|\langle f_L(0)\rangle_{AV}|^2 = 3.2$ mb at 800 MeV/c from Fig. 4, we obtain from Eq. (2.20b) the value $V_I \approx 165$ MeV fm^3, the volume integral of the $K^- n \to \pi^- \Lambda$ interaction appropriate for use in CHUCK. At 720 and 530 MeV/c V_I takes the values 181 and 210 MeV fm^3, respectively.

3. Formalism for Structure Calculations

We consider hypernuclear states produced in the (K^-, π^-) reaction on p-shell target nuclei. The states of lowest excitation energy in the residual hypernucleus are produced when a p-shell neutron is converted into a Λ in the lowest s shell (s_Λ). In line with nuclear structure terminology we call these states, in which s_Λ is coupled to a nuclear p-shell core, $0\hbar\omega$ states. Extensive $0\hbar\omega$ shell-model calculations have been made by Gal, Soper and Dalitz [28] and, where necessary, we use their results for such hypernuclear configurations.

For the K^- beam energies used at BNL and CERN $p_N \to p_\Lambda$ transitions are very strong; these include the substitutional transitions, strongest at 0°, which leave the many-body wave function essentially unchanged (except that a Λ replaces a neutron). Most of the states of the $1\hbar\omega$ configuration $s^4p^n p_\Lambda$ $(n + 5 = A)$ have not yet been resolved or identified because of the relatively crude resolution (of order 2 MeV) and the restriction to small angles. In this paper we perform calculations for such configurations and use the wave functions to provide the spectroscopic input for calculations of the (K^-, π^-) reaction cross sections in order to identify and assign quantum numbers to observed hypernuclear states.

We should also consider $1\hbar\omega$ configurations of the form $s^3p^{n+1}s_\Lambda$ since they can also be formed in the (K^-, π^-) reaction. Because of the high energy and large width of the nuclear s-hole state the resulting hypernuclear states are also expected to be broad and will occur above the states which mainly interest us. It should be realized, however, that the lowest $1\hbar\omega$ hypernuclear states lie below the $s^4p^n p_\Lambda$ configurations of particular interest for the (K^-, π^-) reaction. This is because some $1\hbar\omega$ levels of the nuclear core, to which an s_Λ can couple, always occur at excitation energies lower than the separation between the s_Λ and p_Λ orbits (about 11 MeV). The main effect of these $1\hbar\omega$ core $\otimes s_\Lambda$ configurations, mostly of the form $s^4p^{n-1}(sd)s_\Lambda$, will be to produce some fragmentation of the $0\hbar\omega$ core $\otimes p_\Lambda$ strength. Yet any fragmentation of this sort would not be noticeable with the current experimental resolution in (K^-, π^-) experiments.

Another reason for including $1\hbar\omega$ configurations of the type $1\hbar\omega$ core $\otimes s_\Lambda$ in the $1\hbar\omega$ hypernuclear shell-model space is to ensure proper elimination of spurious center

of mass states. If we treat the hyperon as a distinguishable nucleon in a harmonic oscillator basis then all $s^4p^np_\Lambda$ configurations have an overlap of $A^{-1/2}$ with spurious states. Since this overlap is small and uniform we are satisfied, at the present level of sophistication, to work with a basis $s^4p^np_\Lambda$ configurations only. Calculations for $s_N \to s_\Lambda$ transitions, on the other hand, require a more careful treatment of the center of mass problem, a treatment which is quite feasible with current shell-model techniques.

3.1. *The Shell-Model Calculation*

The hypernuclear Hamiltonian can be written in the form

$$H = H_N + H_Y + V_{NY}, \tag{3.1}$$

where H_N is the Hamiltonian for the nuclear core, H_Y is the single-particle Hamiltonian for the hyperon and V_{NY} represents the residual interaction of the hyperon with the nucleons. We write the shell-model basis states in a weak-coupling representation

$$\{|\alpha_c J_c T_c \otimes j_Y Y; JT\rangle\}, \tag{3.2}$$

where $\alpha_c J_c T_c$ label individual core wavefunctions, which in our case are obtained using the Cohen and Kurath (8–16)POT interaction [15] for H_N, and $j_Y Y$ label the total angular momentum and isospin of the hyperon; J_c and j_Y are coupled to J and similarly for the isospins.

We can always write the two-particle NY interaction in terms of creation and annihilation operators

$$V_{NY} = \sum \hat{K}\hat{T}\langle j_N 1/2 j_Y Y | V | j_N' 1/2 j_Y' Y' \rangle^{KT} |(a^\dagger_{j_N 1/2} \otimes a^\dagger_{j_Y Y})^{KT} \otimes (\tilde{a}_{j_N' 1/2} \otimes \tilde{a}_{j_Y' Y'})^{KT}|^{00},$$

where

$$\hat{j} = (2j+1)^{1/2} \qquad \text{and} \qquad \tilde{a}_{jmtm_t} = (-)^{j+m+t+m_t} a_{j\,-m\,t\,-m_t}. \tag{3.3}$$

On recoupling the operators we have

$$V_{NY} = \sum_\alpha C(\alpha)(\rho^{kt}_{j_N 1/2, j_N' 1/2} \otimes \rho^{kt}_{j_Y Y, j_Y' Y'})^{00}, \tag{3.4}$$

where $\alpha \equiv \{j_N j_N' j_Y j_Y' kt\}$,

$$\rho^{kt}_{j1/2, j'1/2} \equiv (a^\dagger_{j1/2} \otimes \tilde{a}_{j'1/2})^{kt} \tag{3.5}$$

and

$$C(\alpha) = \sum_{KT} \begin{pmatrix} j_N & j_Y & K \\ j_N' & j_Y' & K \\ k & k & 0 \end{pmatrix} \begin{pmatrix} 1/2 & Y & T \\ 1/2 & Y' & T \\ t & t & 0 \end{pmatrix} \hat{K}\hat{T}\langle j_N 1/2 j_Y Y | V | j_N' 1/2 j_Y' Y' \rangle^{KT} \tag{3.6}$$

The unitary $9-J$ symbols effect the recoupling transformation and can be written in terms of $6J$ symbols. For the case of interest here $Y \equiv \Lambda(t=0)$ and

$$C(\alpha) = 1\hat{2}\,\hat{k} \sum_{K} (2K+1)(-)^{j'_N + j_\Lambda + K + k} \begin{Bmatrix} j_N & j_\Lambda & K \\ j'_\Lambda & j'_N & k \end{Bmatrix} \langle j_N j_\Lambda \,|\, V | j'_N j'_\Lambda \rangle^{K1/2}. \tag{3.7}$$

The many-particle matrix elements in a weak-coupling basis can now be written

$$\langle \alpha_c J_c T_c \otimes j_\Lambda ; J | V_{N\Lambda} | \alpha'_c J'_c T_c \otimes j'_\Lambda ; J \rangle$$

$$= \sum_{\alpha} C(\alpha) \begin{pmatrix} J'_c & k & J_c \\ j'_\Lambda & k & j_\Lambda \\ J & 0 & J \end{pmatrix} \langle \alpha_c J_c T_c \| \rho^{k0}_{j_N j'_N} \| \alpha'_c J'_c T_c \rangle \langle j_\Lambda \| \rho^{k0}_{j_\Lambda j'_\Lambda} \| j'_\Lambda \rangle$$

$$= \sum_{\alpha} C(\alpha)\, \hat{J}_c (-)^{J'_c + j_\Lambda + k + J} \begin{Bmatrix} J_c & J'_c & k \\ j'_\Lambda & j_\Lambda & J \end{Bmatrix} \langle \alpha_c J_c T_c \| \rho^{k0}_{j_N j'_N} \| \alpha' J'_c T_c \rangle, \tag{3.8}$$

where we use Brink and Satchler's [19] definition of a reduced matrix element which gives

$$\langle j_\Lambda \| \rho^{k0}_{j_\Lambda j_\Lambda} \| j'_\Lambda \rangle = \hat{k}/\hat{j}_\Lambda . \tag{3.9}$$

The one-body density matrix elements for the nuclear core are calculated for a given nuclear interaction and stored. For any set of ΛN two-body matrix elements the matrix of the hypernuclear Hamiltonian can be very rapidly constructed using (3.8).

3.2. *Spectroscopic Amplitudes for Hypernucleus Formation*

For any inelastic scattering process the structure information is contained in the one-body transition density

$$\langle \alpha_f J_f T_f \| \rho^{k1/2}_{j_\Lambda 0, j_N 1/2} \| \alpha_i J_i T_i \rangle \tag{3.10}$$

with the initial nuclear wave function on the right and the final hypernuclear wave function on the left. Recalling the cross section for the (K^-, π^-) reaction (2.1), (2.17a) and (2.20a) and denoting $T^B_{if} = V^B_I \tilde{T}_{if}$ (this $\tilde{T}_{if}$ was used in our letter [9]) it can be shown that $|\tilde{T}_{if}|^2$ signifies the effective neutron number [10]

$$\overline{|\tilde{T}_{if}|^2} = \langle T_i \tau_i 1/2 1/2 | T_f \tau_f \rangle^2 \frac{2J_f + 1}{2J_i + 1} \sum_{km} \left| \sum_{j_N j_\Lambda} \hat{j}_\Lambda (j_\Lambda \| C^k \| j_N) \times M^{(j_\Lambda j_N)k}_m(E, \theta) \langle \alpha_f J_f T_f \| \rho^{k1/2}_{j_\Lambda 0, j_N 1/2} \| \alpha_i J_i T_i \rangle \right|^2, \tag{3.11a}$$

where the functions $M^{(j_\Lambda j_N)k}_m(E, \theta)$ are proportional to $\beta^k_m(j_\Lambda, j_N)$ of (2.11),

$$\beta^k_m(j_\Lambda, j_N) = V^B_I \hat{k} \hat{j}_\Lambda (j_\Lambda \| C^k \| j_N)\, M^{(j_\Lambda j_N)k}_m, \tag{3.11b}$$

and result from the DWBA integration.

If the single-particle radial wave functions depend only on l_N or l_Λ (e.g., we choose the same binding energy for both j values) the summation over $j_N j_\Lambda$ in (3.11a) can be performed to give

$$\overline{|\tilde{T}_{if}|^2} = \langle T_i \tau_i 1/2 1/2 | T_f \tau_f \rangle^2 \frac{2J_f+1}{2J_i+1}$$

$$\times \sum_k \{2(2l_N+1)\langle l_N 0 k 0 | l_\Lambda 0\rangle^2 N^k(E,\theta)\langle \alpha_f J_f T_f \| \rho^{(k_L k_S)k\,1/2}_{l_N l_\Lambda} \| \alpha_i J_i T_i\rangle^2\} \quad (3.12)$$

with

$$N^k(E,\theta) = \sum_m |M^{(l_N l_\Lambda)k}_m(E,\theta)|^2, \quad (3.13a)$$

where the density matrix element has been transformed from jj to LS coupling and $k_L = k$, $k_S = 0$. For $p_N \to p_\Lambda$ transitions the independent amplitudes N^0, N^2 peak in different angular regions, N^0 falling away rapidly from $\theta_L = 0°$ and N^2 peaking near $\theta_L = 15°$ for the present nuclei and kinematics (see Fig. 7); in fact, in the PW approximation,

$$N^k = \left| \int u_{l_N j_N}(r) j_k(q'r)\, u_{l_\Lambda j_\Lambda}(r)\, dr \right|^2. \quad (3.13b)$$

Equation (3.12) shows that the ratios of cross sections to different final states may be obtained, to a good approximation, by simply squaring the ratio of density matrix elements.

The density matrix elements are readily computed from the nuclear and hypernuclear wave functions. However, it is worthwhile to examine the case where the hypernuclear wave function is simply a weak-coupling state. The transition density (3.10) then becomes

$$\begin{aligned} &\langle p^{n-1}\, \alpha_c J_c T_f \otimes j_\Lambda 0; J_f T_f \| (a^\dagger_{j_\Lambda} \otimes \tilde{a}_{j_N})^{k\,1/2} \| \, p^n \alpha_i J_i T_i\rangle \\ &\quad = \hat{J}_c \hat{k} (-)^{J_i + J_f + k} \begin{Bmatrix} k & J_f & J_i \\ J_c & j_N & j_\Lambda \end{Bmatrix} \langle p^{n-1}\, \alpha_c J_c T_f \| \tilde{a}_{j_N} \| \, p^n \alpha_i J_i T_i\rangle, \end{aligned} \quad (3.14)$$

where the reduced matrix element of the annihilation operator is the product of a factor

$$(-)^{T_f + 1/2 - T_i + J_c + j_N - J_i} \hat{J}_i \hat{T}_i / \hat{J}_c \hat{T}_f$$

and the spectroscopic amplitude for single-nucleon pickup from the target. Thus in the limit of pure weak-coupling the (K^-, π^-) cross section would simply map out the pickup strength. This is seen more clearly if we sum over $J_f j_\Lambda$ assuming again that the DWBA integral depends only on l's, not on j's; expression (3.11a) then assumes the form

$$\sum_k \left[(2k+1)\langle l_N 0k0 | l_\Lambda 0\rangle^2 \sum_j C^2 S_j(c) \right] N^k(E,\theta), \tag{3.15}$$

where S_j is the pickup spectroscopic factor and $C \equiv \langle T_f \tau_f 1/2 - 1/2 | T_i \tau_i \rangle$. For ^{13}C, $C^2 = (2T_f + 1)^{-1}$ and expression (3.15) becomes

$$\frac{1}{2T_f+1} \sum_j S_j N^k(E,\theta) \qquad (\text{for } l_\Lambda = 0, k = 1 \text{ and } l_\Lambda = 1, k = 0), \tag{3.15a}$$

$$\frac{2}{2T_f+1} \sum_j S_j N^2(E,\theta) \qquad (\text{for } l_\Lambda = 1, k = 2). \tag{3.15b}$$

A poor resolution (K^-, π^-) experiment would see just this strength. Regardless of the strength of the coupling or the experimental resolution, (3.15) provides a very useful sum rule. Furthermore summation on J_c yields $n_p N^k(E,\theta)$ for (3.15a) and $2n_p N^k(E,\theta)$ for (3.15), where n_p is the number of p-shell neutrons in the target.

3.3. *Choice of Shell-Model Basis*

In most of our calculations in a $p^n p_\Lambda$ basis we have used the Cohen and Kurath (8–16)POT interaction [15] to generate the wave functions of the nuclear core states. The properties of p-shell levels are generally well described by this interaction. In particular there is no serious disagreement between theory and experiment for spectroscopic factors deduced from single-nucleon pickup and stripping experiments.

In selecting the number of nuclear core states to be used in the construction of the basis for hypernuclear shell-model calculations we have observed two criteria which are to some extent linked:

(a) The core states chosen should to a high degree exhaust the single-nucleon pickup strength from the target.

(b) The core states chosen should account for most of the intensity of configurations with high spatial symmetry.

These requirements ensure that all configurations which can be reached from the target ground state via a one-body operator are included together with configurations of the same supermultiplet symmetry which may admix strongly. To satisfy conditions (a) and (b) for ^{13}C requires at most four core states with the same spin and isospin. It is possible to state the second requirement in the form given, since supermultiplet symmetry (equivalently $SU3$ symmetry) is a good symmetry in the p shell; of the p-shell ground states ^{13}C is the least pure in terms of supermultiplet symmetry with about 70% [441] symmetry. We shall often find it useful to exhibit the spatial symmetry structure of hypernuclear wave functions. For example, in the substitutional reaction in which a Λ particle replaces a neutron with no angular momentum transfer only configurations identical to the target configuration can be reached. Since the target wave function has predominantly one spatial symmetry, in fact a simple LS structure, it is informative to study the hypernuclear wave functions

in this basis also. However, performing the structure calculation in the weak-coupling basis does have the advantage that we can, and do, use the experimental binding energies for the core states. When we cannot make an identification of a calculated core state with an experimental one (this occurs at high excitation energies) we use the theoretical energy in constructing the hypernuclear Hamiltonian matrix. Small shifts in the energies of these core levels have negligible effects on our predictions for excitation strength in the (K^-, π^-) reaction.

3.4. *Parameterization of the Two-Body Interaction*

We use a central interaction of the form

$$V_{N\Lambda} = -V(r)(1 - \varepsilon + \varepsilon P_x)(1 + \alpha \boldsymbol{\sigma}_N \cdot \boldsymbol{\sigma}_\Lambda), \tag{3.16}$$

where P_x is the space exchange operator. For baryons in p orbits the interaction is characterized by two radial integrals commonly denoted by $F^{(0)}$ and $F^{(2)}$. The two-body matrix elements in LS coupling are the product of a spin factor $1 + \alpha(4S - 3)$ and an orbital factor given by

$$\begin{aligned} L &= 0, \quad F^{(0)} + 2/5\, F^{(2)}, \\ L &= 1, \quad (1 - 2\varepsilon)(F^{(0)} - 1/5\, F^{(2)}), \\ L &= 2, \quad F^{(0)} + 1/25\, F^{(2)}. \end{aligned} \tag{3.17}$$

Unless ε is large, $F^{(0)}$ affects mainly the overall binding energy. Dalitz and Gal [29], in their studies of ${}^{9}_{\Lambda}$Be have used $F^{(0)} = -1.16$ MeV and $F^{(2)} = -3.69$ MeV. Bouyssy [30] has obtained $\alpha \approx -0.15$ in fits to CERN data on ${}^{16}_{\Lambda}O$, a value similar to that used by Dalitz and Gal. A value $\varepsilon \approx 0.25$ is consistent with Λ–p elastic scattering data [31] and has been used by Bouyssy. In summary, the $N\Lambda$ interaction seems to be relatively weak (for the p-shell interaction in ordinary nuclei $F^{(2)} \approx -10$ MeV) without any strong exchange dependence.

In addition to the one-body spin–orbit splitting of the p-shell Λ orbits, $\varepsilon_{p_{1/2}} - \varepsilon_{p_{3/2}}$, which we denote by ε_p, we also consider symmetric and antisymmetric two-body spin–orbit interactions

$$v_\pm(r)(\mathbf{s}_\Lambda \pm \mathbf{s}_N) \cdot \mathbf{l}_{N\Lambda}. \tag{3.18}$$

It is sometimes more convenient to write

$$\begin{aligned} &v_\Lambda(r)\, \mathbf{s}_\Lambda \cdot \mathbf{l}_{N\Lambda}, \qquad v_\Lambda(r) = v_+(r) + v_-(r), \\ &v_N(r)\, \mathbf{s}_N \cdot \mathbf{l}_{N\Lambda}, \qquad v_N(r) = v_+(r) - v_-(r). \end{aligned} \tag{3.19}$$

Then the interaction of p_Λ with the closed nuclear s shell gives

$$\varepsilon_p = -3I_1(v_\Lambda), \tag{3.20}$$

where $I_1(v_\Lambda)$ is the diagonal radial integral of $v_\Lambda(r)$ for an $N\Lambda$ relative p state:

$$I_1(v_\Lambda) = \int_0^\infty u_p^2(r)\, v_\Lambda(r)\, dr. \tag{3.21}$$

Calculations of one-body spin–orbit splittings by Dover and Gal [32], which use the baryon–baryon potentials of deSwart *et al.* [33], predict that the Λ-nucleus spin–orbit interaction is much weaker than, and of the same sign as, the N-nucleus spin–orbit interaction. This conclusion is consistent with those of other analyses [34] and with analyses of hypernuclear data [2, 35].

Within the p shell the v_Λ term behaves in part like a one-body interaction. The interaction of p_Λ with the closed p shell gives a contribution to ε_p equal to

$$-3/2\,[I_1(v_\Lambda) + 5I_2(v_\Lambda)], \tag{3.22}$$

where $I_2(v_\Lambda)$ is the radial integral for relative d states. However, v_Λ, as does v_N, also gives rise to other terms including off-diagonal matrix elements in the weak-coupling basis of the shell model.

Interactions based on meson exchange models [32] indicate that $v_+(r)$ should be attractive and $v_-(r)$ repulsive resulting in a weak but attractive $v_\Lambda(r)$ potential. In this case $v_N(r)$ would be attractive and quite strong. The empirical matrix elements obtained by Gal, Soper, and Dalitz [28] in their fit to hypernuclear ground-state binding energies are not consistent with these expectations. Also we know that in determinations of effective interactions in the nuclear p shell there is considerable freedom in the division of the spin–orbit interaction into one- and two-body parts; the empirical two-body spin–orbit matrix elements may be very different from the G-matrix elements derived from NN potentials which fit the two-body scattering data. Consequently we take the point of view that there is very little theoretical guidance as to the form of the $N\Lambda$ spin-orbit interaction and proceed to parametrize the interaction. For short-range spin–orbit interactions we have $I_2(v_\pm) \ll I_1(v_\pm)$ and

$$\langle {}^3P_J | v_+(\mathbf{s}_\Lambda + \mathbf{s}_N)\cdot \mathbf{l}_{N\Lambda} | {}^3P_J\rangle = \begin{cases} -I_1(v_+); & J=0 \\ -1/2\, I_1(v_+); & J=1, \\ 1/2\, I_1(v_+); & J=2 \end{cases} \tag{3.23}$$

$$\langle {}^3P_1 | v_-(\mathbf{s}_\Lambda - \mathbf{s}_N)\cdot \mathbf{l}_{N\Lambda} | {}^1P_1\rangle = -1/\sqrt{2}\; I_1(v_-).$$

For the moment we neglect tensor and quadratic spin–orbit interactions. It is a trivial matter to include them in the structure calculations if, e.g., effective-interaction matrix elements based on realistic baryon–baryon potentials become available.

4. Optical Potentials; Bound State Orbits

Not much data are available for K^- and π^- elastic scattering on p-shell nuclei and of course none for the proper exit π^- channels on hypernuclei. We must in fact make

TABLE I

Potentials for π^- and K^- Elastic Scattering at $p_K = 800$ MeV/c

Potential	Reaction	V_0 (MeV)	W_0 (MeV)	r_0 (fm)	a_0 (fm)	χ^2/N	rms radius (fm)
$K1$	$K^- + {}^{12}C$	24.4	41.4	1.075	0.375	0.31	2.36
$K2$	$K^- + {}^{12}C$	36.17	37.98	1.0	0.5	0.90	2.57
$\pi 1$	$\pi^- + {}^{12}C$	0.9	50.9	0.926	0.44	2.5	2.32
$K3$	$K^- + {}^{40}Ca$	27.04	32.14	1.107	0.57	0.76	3.62
$K4$	$K^- + {}^{40}Ca$	26.34	28.06	1.134	0.55	0.76	3.63
K5	$K^- + {}^{40}Ca$	23.57	18.69	1.182	0.49	0.71	3.62

do with ^{12}C and ^{40}Ca targets for $p_K \approx p_\pi = 800$ MeV/c [12]. The CMU/Houston/BNL collaboration performing such experiments at the Brookhaven AGS has analyzed their data in an optical model framework but using a potential proportional to a Gaussian density [12]. We reanalyze these data here employing the simple Woods–Saxon forms of Eq. (1.5) inserted in a Klein–Gordon equation. Table I presents a list of both K^- and π^- potentials obtained with fit parameters. We do not allow for different real and imaginary geometry but do use slightly different K^- and π^- potentials. Figures 5 and 6 give sample fits along with the data and errors of Ref. [12]. Also included in Table I are the *rms* radii of the various potentials. These radii are very similar for K^- and π^- potentials and indeed are only slightly larger

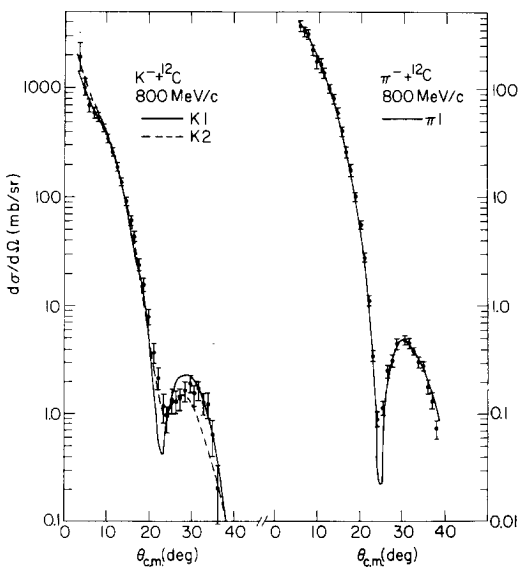

FIG. 5. Optical model fits to the 800-MeV/c elastic scattering data for K^- and π^- mesons incident on ^{12}C. The data are from Marlow *et al.* [12], while the curves labeled K1, K2 and $\pi 1$ refer to the Woods–Saxon potential parameters given in Table I.

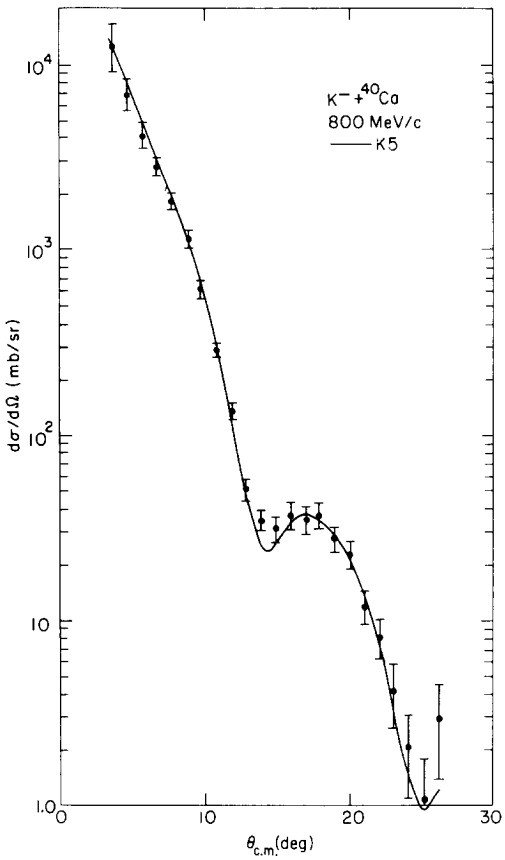

FIG. 6. Optical model fit to the $K^- + {}^{40}Ca$ elastic scattering data of Marlow *et al.* [12] at 800 MeV. The parameters of model $K5$ are given in Table I.

then the point-matter radii deduced from electron scattering. One concludes that the effective K^-N and π^-N interactions are extremely short-ranged, at least at 800 MeV/c projectile momentum.

Potentials $K3$, $K4$ and $K5$ of Table I represent a family of potentials which fit the $K^- + {}^{40}$Ca data of Ref. [12] essentially equivalently. We note the following regularities: (1) as r_0 increases, a decreases and (2) W_0 decreases strongly with increasing r_0; the dominant requirement for a fit appears to be the value of the volume-integrated potential in the surface region.

A rather interesting result of our searches of the π^- and K^- potentials is the determination of the real parts: A qualitative examination of the data in Fig. 5 is helpful. Both π^- and K^- scattering are diffractive, arising from the presence of a well-defined strong absorption. In the absence of a real potential, the first minimum with angle in $\sigma_{\pi A}$ and σ_{KA} would be deep; the real depth is then selected to fill in this minimum appropriately and its sign may be inferred from its effects at more forward angles. In

this way, we deduce a moderately attractive real K^- potential and a small but slightly attractive π^- potential.

We have also carried out calculations using the Gaussian density and parameters of Marlow *et al.* [12] for the initial distorted waves. Peak cross sections for the $^{12}C(K^-, \pi^-)\,^{12}_{\Lambda}C$ reaction are less than those calculated with our potential set $K2$ by 4, 15 and 10% for $\Delta L = 0$, 1 and 2, respectively. Cross sections for potential K1 lie between the above results, differing from the K2 results by about two-thirds of the percentages listed above. These results give some measure of the sensitivity of computed absolute cross sections to changes in the parameters of optical potentials which maintain a satisfactory fit to the elastic scattering data. To describe the (K^-, π^-) reaction we have elected to use the optical potentials $\pi 1$ and $K2$ and scale the radius as $A^{1/3}$ for targets other than ^{12}C. The error inherent in such a procedure is unknown but is probably not larger than other sources of variation in our cross section estimates, such as the choice of single-particle wave functions.

In the zero-range approximation the single-particle wave functions of the neutron and Λ enter the radial integral of Eq. (2.12) as a simple product, often called the form factor. The cross section is influenced by the spatial extent and degree of overlap of the single-particle wave functions. In all cases we have fixed the size of the Woods–Saxon well used to generate the single-particle wave functions at $r_0 = 1.15$ and $a = 0.63$, where the radius is taken as r_0 times $A^{1/3}$ of the bound state core. The depth of the well for a given single-particle orbit is then adjusted to fit the binding energy of the orbit, usually taken as the separation energy corresponding to a particular state of the core. The chosen well geometry ensures that the rms charge radii of the target nuclei are adequately reproduced; the assumption of the same well geometry for neutrons and protons should be good for such light nuclei. We have not included a spin–orbit term in the bound-state potential since the wave function changes due to a spin–orbit potential are small.

The ground-state neutron separation energies for the target nuclei considered and the Λ separation energies for the corresponding hypernuclei are given in Table II. The neutron separation energies show strong, systematic variations with mass number, reflecting the strong space-exchange component in the NN interaction. The Λ separation energies, on the other hand, show a smooth increase with mass number.

TABLE II

Ground-State Neutron and Λ Separation Energies

Target	^{9}Be	^{10}B	^{11}B	^{12}C	^{13}C	^{14}C	^{14}N	^{15}N	^{16}O
B_n(MeV)[a]	1.67	8.44	11.46	18.72	4.95	8.18	10.55	10.83	15.67
B_Λ(MeV)[b]	6.80	8.82	10.24	10.79[c]	11.69	12.17	12.17	13.59	~13[d]

[a] Reference [36].
[b] References [37, 38]; errors on B_Λ are given in the references.
[c] Reference [6].
[d] Estimate from shell-model calculations.

TABLE III

Dependence of (K^-, π^-) Reaction Cross Sections on Single-Particle Binding Energies[a]

Case	B_A (MeV)	$\theta_{c.m.}$ (deg)[b]	B_N(MeV) 1	5	10	18
$p_N \to p_\Lambda\ \Delta L = 0$	0.1	4	584	547	484	410
	1	4	639	632	577	505
	5	4	614	675	659	614
	0.1	10	58.8	96.9	114	122
	1	10	86.6	133	153	163
	5	10	133	190	216	231
$p_N \to p_\Lambda\ \Delta L = 2$	0.1	4	42.9	25.3	17.6	12.2
	1	4	36.7	25.3	19.0	13.9
	5	4	23.9	21.0	17.8	14.4
	0.1	10	70.9	52.0	38.1	26.6
	1	10	69.3	54.2	41.6	30.2
	5	10	51.4	46.0	38.6	30.7
	0.1	16	46.7	51.2	47.1	39.7
	1	16	56.1	61.1	56.6	48.3
	5	16	59.6	65.9	62.7	55.4
Peak angle	0.1		10	13	14	16
	1		11.5	14	15	16
	5		14	16	17	18
$p_N \to s_\Lambda\ \Delta L = 1$	6	4	98.4	93.3	83.4	71.8
	11.6	4	67.0	71.3	68.4	62.7
	18	4	49.7	56.8	57.0	54.6
	6	10	141	157	152	141
	11.6	10	113	132	134	129
	18	10	91.3	112	117	116
	6	16	63.8	90.1	102	108
	11.6	16	65.1	91.4	104	112
	18	16	62.0	87.3	100	107
Peak angle	6		9	10	10	11
	11.6		10	10.5	11	12
	18		10	11	12	12

[a] The quantity listed is $\sigma^{\Delta L}(E, \theta)$, Eq. (4.2), for $E = 446.4$ MeV and is given in $\mu b/sr$.

[b] The lab. angles corresponding to $\theta_{c.m.} = 4,\ 10,\ 16°$ are 3.8, 9.4, 15.0°, respectively. Generally, $\theta_{c.m.} = 1.064\ \theta_{lab}$ is a very good approximation for the angular range of interest.

For s_Λ hypernuclear states built on the ground state of the core the separation energies listed in Table II are used to construct the form factor. A p_Λ orbit is roughly 10 MeV less bound than the s_Λ orbit and therefore lies close to zero binding energy. If the orbit is actually unbound we use a small binding energy of, say, 0.1 MeV. For a hypernuclear state built on an excited state of the core the binding energy of the neutron is the sum of the ground-state separation energy and the excitation energy of the core state but the Λ binding energy is, in the weak-coupling limit, unchanged from the ground-state separation energy.

The effects, on the cross section for the (K^-, π^-) reaction, of varying the bound-state wave functions can be seen in Table III for a ^{13}C target and $E = 446.4$ MeV ($p_K = 800$ MeV/c). The spatial extent of the single-particle wave function varies considerably with binding energy; for $B_N = 0.1$, 1, 5, 10 and 18 MeV the rms radii of p_N orbits are 5.53, 4.23, 3.12, 2.74 and 2.46 fm, respectively. The (K^-, π^-) cross section is large when the overlap of the bound-state wave functions is large and for some intermediate value of binding energy which maximizes the form factor in the surface region of the nucleus. The way in which the angle at which the cross section

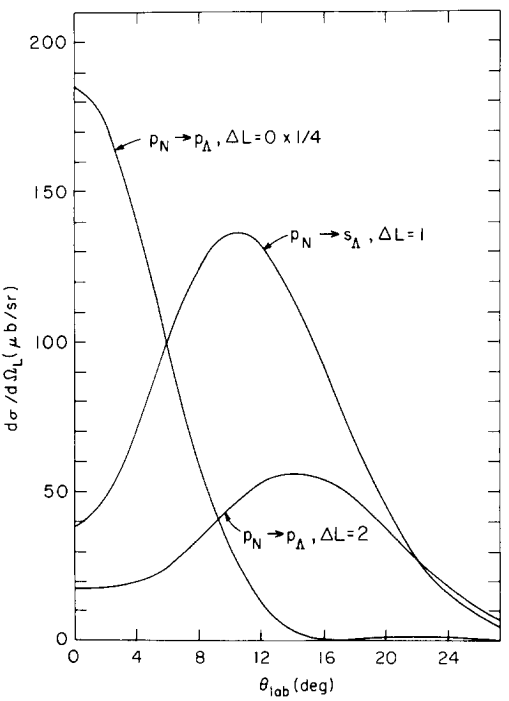

FIG. 7. Laboratory cross sections for the (K^-, π^-) reaction on a ^{13}C target at $p_K = 800$ MeV/c. The curves give $\sigma^{\Delta L}(E, \theta)$ as defined in Eqs. (4.1) and (4.2). The binding energies (in MeV) used are $(B_N, B_\Lambda) = (10, 1)$ for $p_N \rightarrow p_\Lambda$ transitions and (10, 11.6) for $p_N \rightarrow s_\Lambda$ transitions; the radial wave functions for $p_{1/2}$ and $p_{3/2}$ are identical. The excitation energies of the final state are 10 and 0 MeV for $p_N \rightarrow p_\Lambda$ and $p_N \rightarrow s_\Lambda$, respectively.

peaks and the shape of the angular distribution vary as the form factor changes can also be seen from Table III. Full angular distributions for typical choices of form factor are displayed in Fig. 7. Angular distributions for $s_N \to s_\Lambda$ and $p_N \to (sd)_\Lambda$ transitions, which populate states at higher excitation energies in the hypernucleus, are given in Fig. 8.

To enable estimates for (K^-, π^-) cross sections to specific final states to be made, we split the lab cross section, in the spirit of Eqs. (3.11) to (3.13), into products of two factors,

$$\frac{d\sigma}{d\Omega_L} = \sum_k \sigma^k(E, \theta)\, S^k(l_N, l_\Lambda), \tag{4.1}$$

where

$$\sigma^k(E, \theta) = J \frac{k_\pi / k_K}{(2\pi\hbar^2 c^2)^2} \frac{\Pi E_L}{(E_{\text{total}})^2} V_i^2 N^k(E, \theta) \tag{4.2}$$

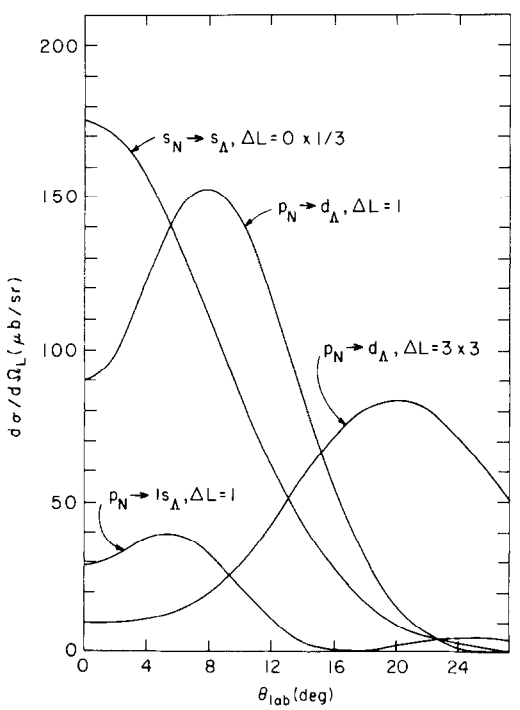

FIG. 8. Same as Fig. 7 for $s_N \to s_\Lambda$ and $p_N \to (sd)_\Lambda$ transitions; $(B_N, B_\Lambda) = (35, 11.6)$ and $(10, 0.1)$, respectively, and a final state excitation energy of 25 MeV in all cases.

and

$$S^k(l_N, l_\Lambda) = \langle T_i \tau_i 1/21/2 | T_f \tau_f \rangle^2 \frac{2J_f + 1}{2J_i + 1} 2(2l_N + 1)$$
$$\times \langle l_N 0k0 | l_\Lambda 0 \rangle^2 \langle \alpha_f J_f T_f \| \rho^{(k0)k1/2}_{l_\Lambda l_N} \| \alpha_i J_i T_i \rangle^2. \tag{4.3}$$

In Eq. (4.2) we have combined the energy factors appearing in Eq. (2.20a) with those of Eq. (2.1). The quantity $\sigma^k(E, \theta)$ for a ^{13}C target is tabulated in Tables III and IV and plotted in Figs. 7 and 8. The "formation strengths," $S^k(l_N, s_\Lambda)$, are given by the coefficients of $N^k(E, \theta)$ in Eq. (3.12). The formation strengths for $\Delta L = 0,2$ transitions to specific final states of the $p^n p_\Lambda$ configuration result from our structure calculations reported in Section 5. These strengths, as well as those for $\Delta L = 1$ to the $p^n s_\Lambda$ configuration, are presented (Figs. 10, 16, 18 to 21) for relevant cases of hypernuclear excitation.

For fixed binding energies the cross sections decrease with increasing mass number; e.g., $p_N \to p_\Lambda$ transitions for $(B_N, B_\Lambda) = (10, 1)$ are larger for ^{9}Be than ^{13}C by 23% for $\Delta L = 0$ at 4° and by 4% for $\Delta L = 2$ at 16°, while for $p_N \to s_\Lambda$ transitions the difference is about 9% at 10°. For more accurate results, particularly where cancellations are involved, the *jj* density matrix elements must be used with the appropriate binding energies to construct the form factor for each contribution to the reaction amplitude.

Finally we give in Table IV a restricted set of cross sections for $p_K = 530$ MeV/c which is close to the "magic" momentum for which the momentum transfer, $p_K - p_\pi$, is zero at 0°; the $\Delta L = 0$ transitions naturally dominate even more strongly in the forward direction than at $p_K = 800$ MeV/c.

TABLE IV

$\sigma^{\Delta L}(E, \theta)$ for $p_K = 530$ MeV/c on ^{13}C

	$\theta_{c.m.}$ (deg)	4°	10°	16°
$p_N \to p_\Lambda$	$\Delta L = 0^a$	708	375	109
$p_N \to p_\Lambda$	$\Delta L = 2^{a,b}$	9.1	12.6	32.8
$p_N \to s_\Lambda$	$\Delta L = 1^{c,d}$	19.8	78.8	113

[a] $(B_N, B_\Lambda) = (10,1)$, B in MeV; $\sigma^{\Delta L}(E, \theta)$ in $\mu b/sr$.
[b] $\Delta L = 2$ cross section peaks at 23° (46.3 $\mu b/sr$).
[c] $(B_N, B_\Lambda) = (10, 11.6)$, B in MeV.
[d] $\Delta L = 1$ cross section peaks at 17° (113 $\mu b/sr$).

5. Results and Discussion

5.1. *The Data*

We consider data taken with the CERN and BNL hypernuclear spectrometers using the (K^-, π^-) reaction on p-shell target nuclei. In the mass range of interest to us, the CERN experiments to date [2–5] have used an incident kaon momentum of 720 MeV/c to study ${}^{6}_{\Lambda}Li$, ${}^{7}_{\Lambda}Li$, ${}^{9}_{\Lambda}Be$, ${}^{12}_{\Lambda}C$ and ${}^{16}_{\Lambda}O$ close to 0° for the emerging π^-. At *BNL*, spectra for ${}^{12}_{\Lambda}C$, ${}^{13}_{\Lambda}C$ and ${}^{14}_{\Lambda}N$ have been obtained [6, 7] at 800 MeV/c and for angles out to 25°.

5.2. *The General Approach*

We perform structure calculations for states in which a Λ particle in a p orbit is coupled to the nuclear core. We use a fixed set of parameters to describe the ΛN interaction for all hypernuclei from ${}^{9}_{\Lambda}Be$ to ${}^{16}_{\Lambda}O$. This should be a good approximation because the size of the core nuclei changes little over the mass range of interest; in fact the measured rms charge radii are constant to within 0.1 fm from ${}^{9}Be$ to ${}^{15}N$. Approaches [15] to the structure of the p-shell nuclei which use an A-independent effective interaction have been very successful. For the lightest p-shell hypernuclei for which data exist, such as ${}^{6}_{\Lambda}Li$ and ${}^{7}_{\Lambda}Li$, we might well expect some change in the effective interaction. In addition it is necessary in such light nuclei to properly eliminate spurious center of mass states. Consequently we restrict our attention to $A \geqslant 9$.

We present results calculated with a standard ΛN interaction; $F^{(0)} = -1.16$ MeV, $F^{(2)} = -3.2$ MeV, $\alpha = -0.1$, $\varepsilon = 0$ and a small spin–orbit splitting $\varepsilon_p = 0.5$ MeV (for $\varepsilon = 0$, $F^{(0)}$ affects only the overall binding energy). We consider the consequences of varying some of the parameters, but it seems that a rather weak, basically Wigner-type central interaction together with a small one-body spin–orbit splitting gives a quite satisfactory explanation of the available data.

The lowest levels in the hypernuclei studied are populated via $p_N \to s_\Lambda$ transitions, more strongly at angles away from the forward direction as the momentum transfer increases. For the $p^n s_\Lambda$ ($n = A$-5) wave functions we use the results of Gal, Soper and Dalitz [17, 28]. In most cases these wave functions are close to the weak-coupling limit. In contrast, the $p^n p_\Lambda$ wave functions often deviate from the pure weak-coupling limit, in the sense that $p_{3/2}$ and $p_{1/2}$ configurations based on the same core state are strongly mixed. It is simply that the hypernuclear wave functions tend towards an LS-coupling structure, a consequence of the basically LS nature of the core wave functions and the absence of strong spin-dependent interactions (particularly the small spin–orbit splitting for p_Λ orbits). There is also a tendency towards good spatial symmetry, realized for the core but not fully developed for the hypernuclear levels because the ΛN interaction is considerably weaker than its NN counterpart. We endeavor in the following analysis of the hypernuclear wave functions to make clear the role played by such symmetries.

5.3. *Individual Nuclei*

5.3.1. *The Hypernucleus* ${}^{13}_{\Lambda}C$

The data from the ${}^{13}C(K^-, \pi^-){}^{13}_{\Lambda}C$ reaction at $p_K = 800$ MeV/c have been presented by May *et al.* [7] and the main results of our calculations appeared in a companion letter [9]. The ${}^{13}_{\Lambda}C^*$ spectrum consists of five main peaks which we refer to as the 0-, 5-, 10-, 16- and 25-MeV peaks. Cross sections were obtained at angles up to 25°; we concentrate on the data at 4 and 15°.

The general features of the data can be simply understood via Eq. (3.15) in terms of the distribution of pickup strength from ${}^{13}C$. This is shown in Fig. 9. By coupling a Λ in an s orbit to the ${}^{12}C$ states in Fig. 9b we expect $\Delta L = 1$ strength ($p_N \to s_\Lambda$ transitions) in the ${}^{13}C(K^-, \pi^-){}^{13}_{\Lambda}C$ reaction at excitation energies of 0, 5 and 12–16 MeV. Coupling a p_Λ to the same set of core states should lead to a repetition of this pattern at excitation energies ~10 MeV higher, the $p_N \to p_\Lambda$ transitions being $\Delta L = 0$ or $\Delta L = 2$ in character. We can also expect $p_N \to (sd)_\Lambda$ and $s_N \to s_\Lambda$ transitions to contribute above $E_x \sim 20$ MeV. Thus, provided the ΛN interaction is not strong enough to give large shifts in these distributions based solely on the pickup strength, the origin of the five peaks in the ${}^{13}_{\Lambda}C^*$ spectrum is qualitatively clear. It is evident that the 16- and 25-MeV peaks do not represent the excitation of single levels. The spectroscopic strengths of individual states in the standard calculation are plotted in Fig. 10. Using this structure input in the DWBA reaction calculation gives a very satisfactory account of the experimental angular distributions (measured out to 25°) for the 10-, 16- and 25-MeV peaks (see Fig. 1 of Ref. [9]). Another way of comparing the theory with the data is presented in Fig. 11. The calculated cross sections for the states shown in Fig. 10 have been folded with Gaussians of width equal to the experimental resolution (2.3 MeV for the bound levels of ${}^{13}_{\Lambda}C$ and arbitrarily 3 MeV for higher levels) and then collected in 1-MeV bins. The resulting histograms are compared directly with the data at 4° and 15°. At forward angles the $\Delta L = 0$ population of $1/2^-$ states dominates; at 15° the $\Delta L = 0$ cross section has fallen to a negligible value while $\Delta L = 1$ transitions populating $1/2^+$ and $3/2^+$ states and $\Delta L = 2$ transitions populating $3/2^-$ and $5/2^-$ states are of comparable importance.

If the agreement between theory based on weak coupling and experiment were perfect within the limitations imposed by the experimental resolution and errors, little could be learned about the ΛN interaction beyond the fact that it is not strong enough to produce any observable departures from pure weak coupling. Information on the detailed structure of the hypernuclear states comes primarily from the energies and cross sections of the 10- and 16-MeV peaks at 4° and 15°. The interesting features of the 10- and 16-MeV peaks, which signal a departure from weak coupling, are summarized as follows.

(i) The cross section ratio of the two peaks at 4°, $\rho = \sigma(1/2^-_>)/\sigma(1/2^-_<) \simeq 5.5$, deviates strongly from the pickup ratio whether taken from experiment [39],

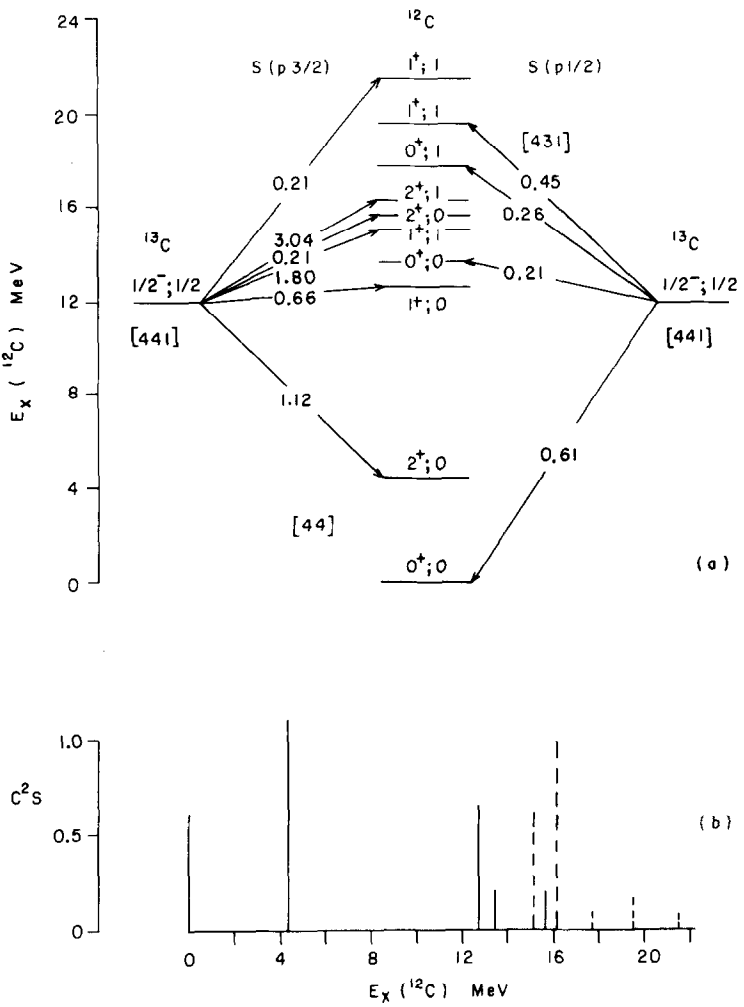

FIG. 9. (a) Spectroscopic factors for $p_{3/2}$ and $p_{1/2}$ pickup from ^{13}C calculated using Cohen and Kurath's (8–16)POT interaction [15]. $S > 0.2$ are shown. For the five strongest states there is good agreement with the experimental values [39]. The dominant spatial symmetries of the ^{13}C ground state and of the two groups of ^{12}C states are indicated.

(b) C^2S plotted as a function of excitation energy in ^{12}C; $C^2 = 1/(2T + 1)$, where T is the isospin of the ^{12}C level and S is the sum of the spectroscopic factors for $p_{1/2}$ and $p_{3/2}$ pickup. Solid lines are for $T = 0$ states, dashed lines for $T = 1$. C^2S is directly related to the sum rule strength in the (K^-, π^-) reaction by Eq. (3.15).

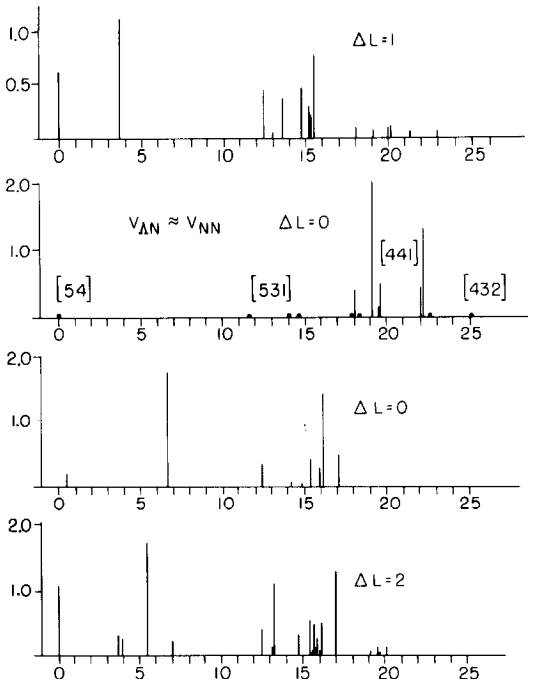

FIG. 10. Formation strengths, Eq. (4.3), for ${}^{13}_{\Lambda}C$ states (the appropriate sum rule values are 5 for $\Delta L = 0,1$ and 10 for $\Delta L = 2$), by which $\sigma^{\Delta L}(E, \theta)$ of Eq. (4.2) must be multiplied to give the differential cross section. Excitation energies are given relative to the lowest $p^8 s_\Lambda$ or $p^8 p_\Lambda$ state. To compare the $\Delta L = 1$ strength with the $\Delta L = 0$ or $\Delta L = 2$ strength a shift of $\sim$10 MeV representing the energy separation between s_Λ and p_Λ single-particle states in the Λ-nucleus potential must be applied. The distribution of $\Delta L = 0$ strength for $V_{NN} \approx V_{N\Lambda}$ is also shown. The dots mark the location of states with negligible formation strength; the various spatial symmetries dominate in the regions indicated.

$\rho(p, d) = 1.45$ and $\rho(d, t) = 1.77 - 1.98$, or from intermediate coupling calculations [15], $\rho(CK) = 1.83$.

(ii) The 6.0 ± 0.4-MeV spacing between the two peaks at 4° clearly deviates from the 4.4-MeV spacing of the corresponding ${}^{12}C$ core states. Ignoring the ΛN residual interaction leads to a negative Λ-nucleus spin–orbit splitting $\varepsilon_p = -1.6 \pm 0.4$ MeV.

(iii) The 16-MeV peak undergoes a downward shift of 1.7 ± 0.4 MeV in going from 4° to 15°. After subtraction, at 15°, of the $\Delta L = 1\ p_N \rightarrow s_\Lambda$ transitions (a procedure which little affects this shift), the remaining $\Delta L = 2\ p_N \rightarrow p_\Lambda$ transitions within this peak are dominated (90%) by $5/2^-$ states of the ${}^{12}C(2^+) \otimes p_\Lambda$ configuration. Ignoring the ΛN residual interaction again leads to a negative value for ε_p, of about the same magnitude as that inferred in (ii).

(iv) The 10-MeV peak undergoes only a small downward energy shift of 0.36 ± 0.3 MeV in going from 4° to 15°, corresponding in the weak-coupling limit to

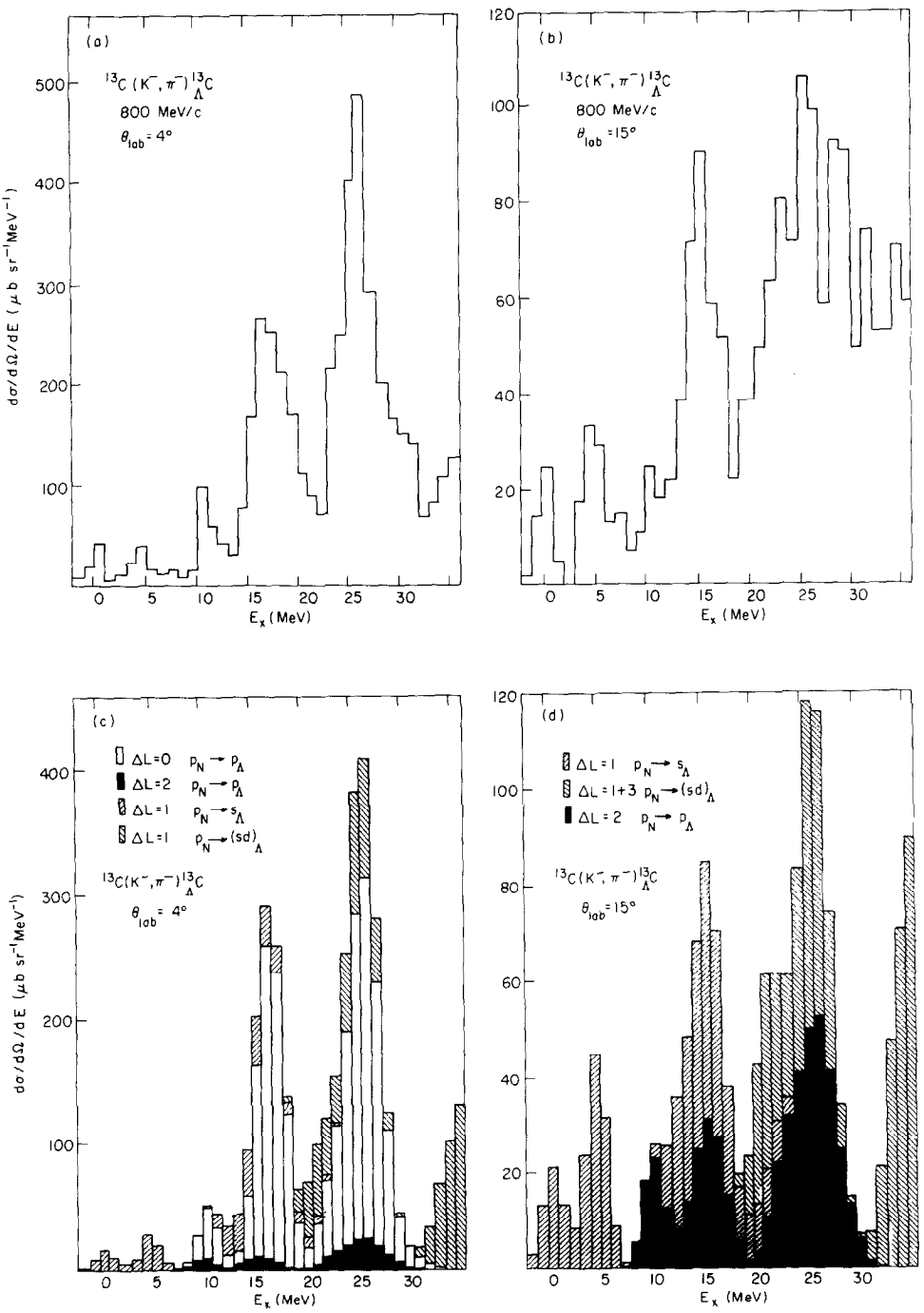

FIG. 11. Direct comparison between the $^{13}C(K^-,\pi^-)^{13}_{\Lambda}C$ data and theory for laboratory angles of 4° and 15°. See text.

$^{12}C(0^+) \otimes p_{1/2\Lambda} \rightarrow {}^{12}C(0^+) \otimes p_{3/2\Lambda}$ and thus resulting in a small positive spin–orbit splitting $\varepsilon_p = 0.36 \pm 0.3$ MeV. This feature apparently contradicts the previous two features when analyzed in the weak-coupling limit, which is therefore inappropriate: a nonvanishing ΛN residual interaction is imposed by the ${}^{13}_{\Lambda}C$ data.

(v) The 4° data shows three peaks, the 10-, 16- and 25-MeV peaks, which we interpret as being populated by $p_N \rightarrow p_\Lambda$, $\Delta L = 0$ transitions. This is evidence that the ΛN interaction is considerably weaker than the NN interaction since for $V_{\Lambda N} \approx V_{NN}$ all the $p_N \rightarrow p_\Lambda$, $\Delta L = 0$ strength would appear, as the p-shell part of the strangeness analog state, in a single peak (see Fig. 10).

The essential features of the ${}^{13}_{\Lambda}C$ spectrum are obtained for an interaction with no dependence on the spin of the Λ particle. Beginning with

$$\mathbf{J} = \mathbf{J}_c + \mathbf{j}_\Lambda, \qquad \mathbf{j}_\Lambda = \mathbf{l}_\Lambda + \mathbf{s}_\Lambda \tag{5.1}$$

we can change to a coupling scheme specified by

$$\mathbf{J} = \mathscr{L} + \mathbf{s}_\Lambda, \qquad \mathscr{L} = \mathbf{J}_c + \mathbf{l}_\Lambda. \tag{5.2}$$

For an interaction independent of s_Λ, $\mathscr{L}$ is a good quantum number and doublet degeneracies corresponding to $\mathbf{J} = \mathscr{L} + \mathbf{s}_\Lambda$ arise, independent of the strength of the ΛN interaction and the size of the nuclear core basis. An understanding of features (i)–(v) listed for the 10- and 16-MeV peaks is obtained from the $^{12}C(0^+, 2^+) \otimes p_\Lambda$ spectrum, which is shown in Fig. 12 for $F^{(2)} = -3$ MeV, $\varepsilon = 0$, $\alpha = 0$ and $\varepsilon_p = 0$ MeV. Note that the splitting of the doublets remain small for the spin dependence of our standard interaction, i.e., $\alpha = -0.1$ and $\varepsilon_p = 0.5$ MeV. To discuss the wave functions of the states in Fig. 12, it is first convenient to construct states of good $\mathscr{L}$ in terms of the original weak coupling basis states; transforming from the basis expressed by Eq. (5.1) to that of Eq. (5.2) we have

$$|(\mathscr{L} s_\Lambda) J\rangle = \sum_{j_\Lambda} U(J_c 1 J 1/2, \mathscr{L} j_\Lambda) |(J_c j_\Lambda) J\rangle. \tag{5.3}$$

For the $\mathscr{L} = 1$ states ($J = 1/2, 3/2$) in Fig. 12 there is ~9% mixing of the states with $J_c = 0$ and $J_c = 2$. The wave functions for the standard interaction, given in Table V, show small departures from the good $\mathscr{L}$ limit of Eq. (5.3).

The two ^{12}C core states have dominantly [44] spatial symmetry (79 and 88% for $J_c = 0$ and $J_c = 2$, respectively) and thus intrinsic spin $S_c = 0$. Consequently terms in the ΛN interaction which depend on $\mathbf{s}_N$ such as the tensor interaction and the spin–spin component of the central interaction have little influence on the states of Fig. 12. For a spin-independent Wigner residual interaction between p-shell baryons, all splittings and relative shifts are given in terms of the Slater integral $F^{(2)}$ which determines the strength of a quadrupole–quadrupole effective interaction

$$V_{\text{eff}}(\Lambda N) \sim F^{(2)} Q_N \cdot Q_\Lambda, \qquad Q_B = C^2(\hat{r}_B). \tag{5.4}$$

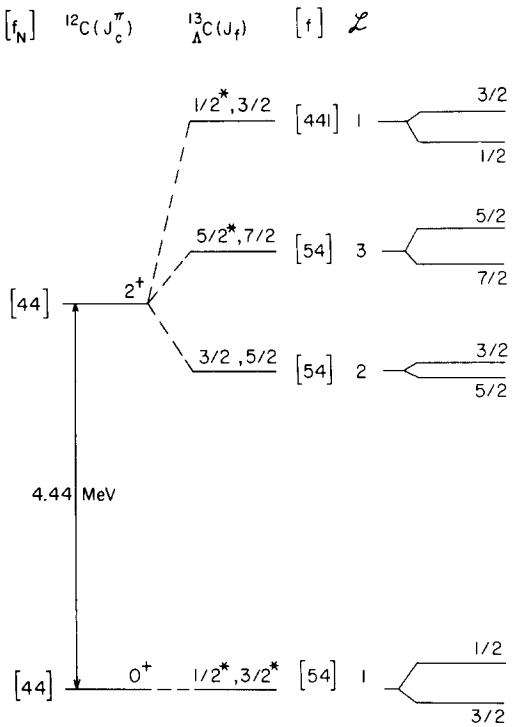

FIG. 12. $^{12}C(0^+, 2^+) \otimes p_\Lambda$ spectrum for an interaction independent of σ_Λ. States which dominate in the 10- and 16-MeV peaks at 0° and 15° are marked with asterisks. $\mathscr{L} = \mathbf{J}_c + \mathbf{l}_\Lambda$ is a good quantum number and the indicated degeneracies result, independent of the size of the nuclear core basis. The dominant spatial symmetry for each state is also given. At the right the doublet splittings resulting from the spin-dependent components of our standard interaction are shown.

TABLE V

Wave Functions of Lowest $p^8 p_\Lambda$ States

		Basis configuration			
J_n^π	E_x (MeV)	$0^+ \otimes p_{1/2\Lambda}$	$0^+ \otimes p_{3/2\Lambda}$	$2^+ \otimes p_{1/2\Lambda}$	$2^+ \otimes p_{3/2\Lambda}$
$3/2_1^-$	9.73		0.963	0.183	−0.198
$1/2_1^-$	10.20	0.956			−0.294
$5/2_1^-$	13.45			0.352	−0.935
$3/2_2^-$	13.59		−0.029	−0.658	−0.751
$5/2_2^-$	15.24			0.927	0.346
$1/2_2^-$	16.39	0.294			0.951
$3/2_3^-$	16.75		0.268	−0.728	0.627

Also, in the limit of a pure LS-coupling state with $L_c = J_c$ and $S_c = 0$, $\mathscr{L}$ becomes the orbital angular momentum of the hypernuclear state and s_Λ the intrinsic spin. Then the energy shifts of states with different L based on the 2^+ state of the core are given by

$$\begin{aligned}\Delta E &= k\langle (L_c l_\Lambda) L \,\|Q_c \cdot Q_\Lambda\| (L_c l_\Lambda) L\rangle \\ &= k\sqrt{5}\begin{pmatrix} 2 & 2 & 2 \\ 1 & 2 & 1 \\ L & 0 & L \end{pmatrix}\langle 2\|Q_c\|2\rangle\langle 1\|Q_\Lambda\|1\rangle \\ &= k'(-)^L \begin{Bmatrix} 2 & 2 & 2 \\ 1 & 1 & L \end{Bmatrix},\end{aligned} \tag{5.5}$$

where k, k' are constants proportional to $F^{(2)}$. Thus the relative energy shifts for $L = 1, 2, 3$ are in the ratios $7: -7: 2$. Taking into account the repulsion of the two $L = 1$ states leads to the structure displayed in Fig. 12.

Another useful way of exhibiting the structure of the states in Fig. 12 is in an LS basis with good spatial symmetry. By coupling a p_Λ particle to a p-shell core with spatial symmetry $[f] = [44]$ we can obtain configurations with $[f] = [54]$ and $[441]$ or equivalently $SU3$ symmetry $(\lambda\mu) = (14)$ and (03). For $[f] = [54]$, $L = 1, 2, 3, 4, 5$ are allowed while for $[f] = [441]$, $L = 1, 3$. The parentages of the $[54]$ states with $L = 1, 3$ are

$$\begin{aligned}|[54]\, L = 1\rangle &= \sqrt{7/9}\,|L_c = 0 \otimes p_\Lambda\rangle - \sqrt{2/9}\,|L_c = 2 \otimes p_\Lambda\rangle, \\ |[54]\, L = 3\rangle &= \sqrt{6/7}\,|L_c = 2 \otimes p_\Lambda\rangle - \sqrt{1/7}\,|L_c = 4 \otimes p_\Lambda\rangle.\end{aligned} \tag{5.6}$$

The $[441]$ states with $L = 1, 3$ are the orthogonal linear combinations. Thus in the LS limit ($L = \mathscr{L}$), the doublet in Fig. 12 with $\mathscr{L} = 2$ has purely $[54]$ symmetry, the lowest $\mathscr{L} = 1$ doublet and the $\mathscr{L} = 3$ doublet have predominantly $[54]$ symmetry and the upper $\mathscr{L} = 1$ doublet has mainly $[441]$ symmetry. The $[54]$ symmetry is not allowed for nine nucleons and hence cannot be reached in the substitutional (K^-, π^-) reaction on ^{13}C. However, the upper $J = 1/2$ state, which has the same symmetry as the ^{13}C ground state in the LS limit, can be reached and should therefore be populated much more strongly at 0° by $\Delta L = 0$ excitation than the lower $J = 1/2$ state. Indeed for the standard interaction we have, in a mixed notation where $|\,^{13}C$ g.s.$\rangle$ stands for the substitutional ^{13}C ground state,

$$\begin{aligned}|1/2_1^-\rangle &= 0.880|[54]\, L = 1 S = 1/2\rangle - 0.145|\,^{13}C \text{ g.s.}\rangle + \cdots, \\ |1/2_2^-\rangle &= -0.189|[54]\, L = 1 S = 1/2\rangle - 0.437|\,^{13}C \text{ g.s.}\rangle + \cdots.\end{aligned} \tag{5.7}$$

Note that the ^{13}C g.s. has only 20% parentage to the 0_1^+ and 2_1^+ core states (Fig. 9). As the strength of the ΛN interaction is increased the symmetry of the lowest $1/2^-$ state becomes more purely $[54]$ corresponding to stronger mixing of the $0^+ \otimes 1/2^-$

and $2^+ \otimes 3/2^-$ weak-coupling basis states (and a small admixture of higher weak-coupling states). Then the hypernuclear states are ordered strictly according to their spatial symmetry[2] and the $\Delta L = 0$ formation strength resides in a cluster of states over which the [441] symmetry is distributed (see Fig. 10). For a weak ΛN interaction, however, the formation strength associated with the [44] and [431] symmetries of the core remains widely separated in energy and the observed separation of the 16- and 25-MeV peaks in the data clearly places a strong constraint on the magnitude of $F^{(2)}$ (see Fig. 3 of Ref. [9]).

States in 10- and 16-MeV peaks with appreciable (K^-, π^-) cross section at 4° $(1/2^-)$ and 15° $(3/2^-, 5/2^-)$ are marked with asterisks in Fig. 12. The actual LS-coupled density matrix elements determine the population strengths $S^k(l_N, l_\Lambda)$ according to Eq. (4.3) and the latter, and are given in Fig. 10. The density matrix elements may be calculated from the wave functions listed in Table V and the pickup spectroscopic amplitudes. However, it is instructive to calculate them for $\Delta L = 2$ in the LS limit with good $SU3$ symmetry, i.e.,

$$\langle (04)_c \times (10)_\Lambda \to (\lambda\mu)\, L\ 1/2\, J \| (a_\Lambda^\dagger \tilde{a}_N)^{(11)202} \| (03)_N L = 1 S = 1/2\, J = 1/2 \rangle$$

$$= \text{const.} \begin{pmatrix} 1 & 2 & L \\ 1/2 & 0 & 1/2 \\ 1/2 & 2 & J \end{pmatrix} \langle (03)\, 1 (11)\, 2 \| (\lambda\mu)\, L \rangle \begin{pmatrix} (03) & (01) & (04) \\ (00) & (10) & (10) \\ (03) & (11) & (\lambda\mu) \end{pmatrix}. \qquad (5.8)$$

The $SU3$ 9-$(\lambda\mu)$ coefficient takes the values 1, $1/\sqrt{2}$ for $(\lambda\mu) = (14)$, (03); the $SU3 \supset R3$ coefficient the values $-\sqrt{9/20}$, $-\sqrt{1/5}$, $\sqrt{7/20}$, $\sqrt{7/40}$, $\sqrt{3/5}$ for $(\lambda\mu)\, L = (03)\, 1$, $(03)\, 3$, $(14)\, 1$, $(14)\, 2$, $(14)\, 3$; the $9J$ coefficient the values $1/\sqrt{2}$, $1/\sqrt{2}$ for $J = 3/2$, $L = 1, 2$ and $\sqrt{2/9}$, $\sqrt{7/9}$ for $J = 5/2$, $L = 2, 3$. Equation (5.8) correctly predicts the general features apparent in Fig. 10 (although it is only good to within a factor of 2 for ratios of some pairs of states). In particular it is clear that the $\mathscr{L} = 3$, $5/2^-$ state should be dominant in the 16-MeV peak at 15°, thus accounting for the downward shift of the 16-MeV peak as the angle changes from 4° to 15°. All measured energy separations, including the 9.3 ± 0.5 MeV between the 16- and 25-MeV peaks at 4°, can, in fact, be accounted for with $-3.4 < F^{(2)} < -3.0$ and $\varepsilon_p = 0.5$ MeV (see Fig. 3 of Ref. [9]). The essential effects of $F^{(2)}$ and ε_p can be readily deduced from Fig. 12 and Table V. The *strict degeneracy* of the lowest $1/2^-$ and $3/2^-$ levels in the absence of interactions which depend on $\mathbf{s}_\Lambda$ means that the measured separation places a *strong constraint* on the *combination* of one- and two-body spin–orbit forces. The energy separation goes as $0.88\varepsilon_p$ for $F^{(2)}$ near its optimum value. For a two-body spin–orbit interaction which reproduces the effect of ε_p in the diagonal elements of the energy matrices, the resultant energy separation is much less. This is because in an open-shell hypernucleus $I_1(v_\Lambda)$ also contributes to off-diagonal matrix elements; for $I_1(v_\Lambda) < 0$ (equivalent to $\varepsilon_p > 0$) the off-diagonal

[2] For $V_{\Lambda N} = V_{NN} \sim Q \cdot Q$ we have $E \sim 4[\lambda^2 + \mu^2 + \lambda\mu + 3(\lambda + \mu)] - 3L(L+1)$ and, e.g., then $(03)\, L = 1$ state lies between the $L = 4$ and $L = 5$ states of the (14) band.

matrix element in the 2×2 matrix for $J^\pi = 1/2^-$ is increased while in the 3×3 matrix for $J^\pi = 3/2^-$ the opposite effect occurs. If the effective interaction is to be determined empirically, there are no particular restrictions on the nature of the spin-orbit interaction. In fact the interplay of one- and two-body spin–orbit interactions in fitting energy level data is familiar from studies in the nuclear p shell. However, if we take seriously our earlier discussion of the origin of the one-body spin–orbit force we would use a predominantly one-body spin–orbit force in our $p^n p_\Lambda$ calculations. Since the $1/2_1^-$ and $3/2_1^-$ levels lie below the lowest particle threshold in ${}^{13}_{\Lambda}C$ (${}^{12}C + \Lambda$ with $B_\Lambda = 11.69 \pm 0.12$ MeV) they should decay predominantly by γ rays to the ${}^{13}_{\Lambda}C$ ground state and their energy separation might be best determined by detecting the 10-MeV γ rays in coincidence with the outgoing pion from the (K^-, π^-) reaction on ${}^{13}C$.

We have demonstrated (Ref. [9] and above) that the observed excitation energies and formation cross sections of states in ${}^{13}_{\Lambda}C$ can be adequately described by an appropriate choice of $F^{(2)}$ and ε_p with $F^{(0)}$ and α being fixed at previously determined values. We now consider the effect of other parameters in the effective interaction such as the space exchange mixture ε in the central force and the two-body spin–orbit force. The quantity most sensitive to parameter changes is the cross section of the lowest $1/2^-$ state, conveniently studied as the ratio R of the formation strengths for the upper and lower $1/2^-$ states in Fig. 12. In the spirit of Eq. (3.12) we take for this quantity the ratio of squares of transition density matrix elements. The full reaction calculation, taking into account distortions and binding energy effects in the form factor, gives a value for $R(\theta_{\text{c.m.}} = 4°)$ somewhat smaller ($R = 6.6$)[3] than that estimated from the density matrix elements alone ($R = 9.1$). If we write the wave function of the lowest $1/2^-$ state as

$$|1/2_1^-\rangle = \gamma |0^+ \otimes p_{1/2}\rangle - \beta |2^+ \otimes p_{3/2}\rangle \tag{5.9}$$

then we have

$$R = \left[\frac{\beta\theta(1/2) + \gamma\theta(3/2)}{\gamma\theta(1/2) - \beta\theta(3/2)} \right]^2, \tag{5.10}$$

where $\theta(1/2)$ and $\theta(3/2)$ are the spectroscopic amplitudes for pickup from the ${}^{13}C$ ground state to the 0^+ and 2^+ states of ${}^{12}C$, respectively. For the small β of interest R is a rapidly varying function of β as shown in Fig. 13. It is clear that R is also sensitive to the details of the core wave functions; for the (8–16) POT interaction [15] $\theta(1/2)$, $\theta(3/2) = -0.783$, -1.059, while for the MP4 interaction [16], which represents a move toward jj coupling, the corresponding values are -0.849, -1.037. Given a model for the core, R is governed by β and thus largely by the off-diagonal matrix element in the $J = 1/2$ energy matrix. This matrix element is dominated by

[3] To compare theoretical and observed cross section ratios we must include calculated $\Delta L = 1$ and $\Delta L = 2$ contributions in the theoretical cross sections. At 4° this leads to a reduction in the effective value of R from that with $\Delta L = 0$ only.

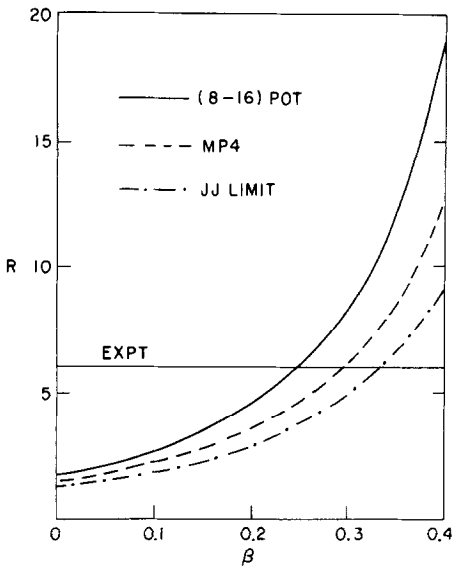

FIG. 13. The ratio R of Eq. (5.10) displayed as a function of the mixing amplitude β of Eq. (5.9) for several models of the ^{12}C core.

$F^{(2)}$. A negative value of α decreases the matrix element but the effectiveness of the $\mathbf{s}_N \cdot \mathbf{s}_\Lambda$ interaction is limited by the dominantly spin-singlet nature of the core wave functions. A space-exchange interaction which weakens the odd state interaction ($\varepsilon > 0$) naturally leads to purer [54] symmetry for the $1/2_1^-$ wave function, i.e., increases the off-diagonal matrix element. There exists evidence [31] for such a component ($\varepsilon \sim 0.25$) in the free Λp interaction. The effectiveness of such a component depends on the range of the interaction, through the combination $F^{(0)} - 1/5F^{(2)}$, and must clearly have no effect for a delta function interaction. Finally the two-body spin–orbit interactions, characterized by the integrals $I_1(v_+)$ and $I_1(v_-)$, increase the off-diagonal matrix element if they are attractive. An interaction derived in a meson-exchange model possesses all such components, and a tensor force besides. A G- matrix calculated from the meson-exchange interaction can be used in the shell-model calculation and an attempt to derive the ΛN effective interaction in this way is clearly a desirable step in the study of Λ hypernuclei. However, in our attempts to obtain an empirical ΛN interaction we are clearly limited in the number of parameters that we can determine by fitting the current set of data. We could probably, for example, have included a space-exchange interaction, fixing $\varepsilon = 0.25$, say, and used $F^{(2)}$ and ε_p to fit the data, paying only the price of a smaller formation cross section for the lowest $1/2^-$ level.

5.3.2. *The Hypernucleus* $^9_\Lambda Be$

The $^9Be(K^-, \pi^-)\,^9_\Lambda Be$ reaction at 0° has been studied at CERN, originally at $p_K =$ 900 MeV/c [1] and later at $p_K = 720$ and 790 MeV/c [2–5]. An unresolved group

consisting of the ${}^{9}_{\Lambda}Be$ ground state ($B_\Lambda = 6.7$ MeV) and states of an s_Λ coupled to the 2.9-MeV 2^+ state of the ${}^{8}Be$ core is observed. The 0° spectrum is dominated by two strong excitations at $-B_\Lambda = 6$–7 MeV and $-B_\Lambda = 17$–18 MeV, respectively. The structure of ${}^{9}_{\Lambda}Be$ which underlies these strong $\Delta L = 0$ excitations has been studied in detail by Dalitz and Gal [29].

In many respects the structure of ${}^{9}_{\Lambda}Be$ is similar to that of ${}^{13}_{\Lambda}C$ since the LS structure of the p^4 core with [4] and [31] symmetries resembles that of the p^8 core with [44] and [431] symmetries. The pickup strength (mostly $p_{3/2}$) goes to the ${}^{8}Be$ g.s., the 2.94-MeV 2^+ state and to a group of states between 16- and 20-MeV excitation energy, particularly the isospin mixed 2^+ states at 16.63 and 16.93 MeV and the 3^+ levels just above 19 MeV [40]. In our description of the core states and the ^{9}Be g.s. we have followed Cohen and Kurath [15] and used the (6–16) 2 BME interaction. Experimental excitation energies are taken from Ajzenberg–Selove's tabulation [40] supplemented by some additional information on $T = 1$ states [41].

A discussion of the ${}^{8}Be$ (0^+, g.s.; 2^+, 2.94 MeV) $\otimes p_\Lambda$ states is instructive, particularly in comparison with the analogous structure in ${}^{13}_{\Lambda}C$, shown in Fig. 12. In ^{8}Be the 0^+ and 2^+ states have very pure spatial symmetry [4] configurations (much smaller $S = 1$ admixtures than in ${}^{12}C$). The hypernuclear states can have [5] or [41] symmetry with $(\lambda\mu)L$ equal to (50) 1, 3, 5 for the former and (31) 1, 2, 3, 4 for the latter (if we include also the 4^+, 11.4-MeV core state). The weak-coupling structure of the ${}^{9}_{\Lambda}Be$ states differs from that of the ${}^{13}_{\Lambda}C$ states because the ${}^{8}Be$ core is prolate, $(\lambda\mu) = (40)$, while the ${}^{12}C$ core is oblate, $(\lambda\mu) = (04)$. Consequently $\langle p^4 \| Q \| p^4 \rangle$ is opposite in sign to $\langle p^8 \| Q \| p^8 \rangle$ and by Eq. (5.5) the order of the $\mathscr{L} = 1, 2, 3$ states based on the 2^+ core state is inverted from that displayed in Fig. 12, with the $\mathscr{L} = 1$ state lowest. The strong interaction between the two $\mathscr{L} = 1$ states then drives the upper $\mathscr{L} = 1$ state to a position between the $\mathscr{L} = 3$ and $\mathscr{L} = 2$ states. A similar result has been obtained in $\alpha + \alpha + \Lambda$ cluster model calculations [42]. In analogy to Eq. (5.6) we have

$$\begin{aligned} |[5]\, L = 1\rangle &= \sqrt{7/15}\, |\, L_c = 0 \otimes p_\Lambda\rangle - \sqrt{8/15}\, |\, L_c = 2 \otimes p_\Lambda\rangle, \\ |[5]\, L = 3\rangle &= \sqrt{27/35}\, |\, L_c = 2 \otimes p_\Lambda\rangle - \sqrt{8/35}\, |\, L_c = 4 \otimes p_\Lambda\rangle \end{aligned} \tag{5.11}$$

so that the mixing of states based on the 0^+ and 2^+ core states will be stronger in ${}^{9}_{\Lambda}Be$ than in ${}^{13}_{\Lambda}C$ as the limit of good spatial symmetry is approached. Even for $F^{(2)} = -3.2$ MeV this mixing is sufficiently strong to make the 0° (K^-, π^-) cross section to the lowest $3/2^-$ state unobservably small relative to that of the second $3/2^-$ state. The remaining $\Delta L = 0$ strength is concentrated in two states with $T = 0, 1$ (probably strongly isospin mixed) about 12.5 MeV above the second $3/2^-$ level. This is in excellent agreement with the calculations of Dalitz and Gal [29], based on pure LS core states, and with the data [4, 5] which show two strong peaks about 12 MeV apart.

Although no data exist as yet for reaction angles away from the forward direction, it is interesting to inquire into the distribution of $p_N \to p_\Lambda$ $\Delta L = 2$ strength, which, starting with the ${}^{9}Be$ g.s. spin of 3/2, can populate hypernuclear states with $J = 1/2$,

3/2, 5/2, 7/2. At 15°, say, the lowest $1/2^-$ and $3/2^-$ states should be populated giving rise to a peak near $B_\Lambda \sim -2.5$ MeV. About 4 MeV above should be a peak, essentially unshifted from the peak in the 0° spectrum and somewhat broadened, consisting of six unresolved levels (with $7/2_1^-$, $5/2_1^-$, $1/2_2^-$ and $3/2_3^-$ strongest). The centroid of $\Delta L = 2$ strength associated with the highly excited core states should be about 1.5 MeV higher than the $\Delta L = 0$ strength, but broadening due to fragmentation will probably make this shift unobservable. Thus the basic differences from the ${}^{13}_{\Lambda}C$ spectrum are the absence of the lowest $\Delta L = 0$ peak and the prediction of no shift with angle for the peak at $-B_\Lambda \approx 6$–7 MeV. Another difference is that the $\Delta L = 1$ strength from an s_Λ coupled to the highly excited core states should occur around $B_\Lambda \approx -10$ MeV and could possibly be resolvable from the $\Delta L = 2$ strength at lower excitation energies (rather than coincident with it as is the case for ${}^{13}_{\Lambda}C$). A measurement at 15° with good energy resolution to determine, in particular, the separation in energy of the two lowest $\Delta L = 2$ peaks would provide a useful constraint on the values of $F^{(2)}$ and ε, the space-exchange mixture.

5.3.3. *The Hypernucleus* ${}^{16}_{\Lambda}O$

The ${}^{16}O(K^-, \pi^-){}^{16}_{\Lambda}O$ reaction at 0° has been studied at CERN, the cleanest spectrum being taken at $p_K = 715$ MeV/c [2]. The spectrum shows four distinct peaks. The peaks at $B_\Lambda = 13$ and $B_\Lambda = 7$ MeV are interpreted [2, 35] as $\Delta L = 1$ excitations of states formed by coupling an s_Λ to the $p_{1/2}^{-1}$ and $p_{3/2}^{-1}$ neutron hole states of ${}^{15}O$. Similarly the stronger peaks at $B_\Lambda = 2.5$ and $B_\Lambda = -3.5$ MeV are interpreted [2, 35] as $\Delta L = 0$ excitations of $(p_{1/2}^{-1}p_{1/2})$ and $(p_{3/2}^{-1}p_{3/2})N^{-1}\Lambda$ configurations. Limited angular distributions [2] are consistent with this interpretation. The approximately 6-MeV separation of the two 0^+ states led to the important conclusion [2, 35] that the Λ-nucleus spin–orbit interaction is very small. This conclusion remains when the effects of the ΛN residual interaction are taken into account [30].

With our standard set of parameters the separation of the two 0^+ states is 6.15 MeV. The mixing of the weak-coupling basis states is very small, only 0.09 in amplitude (β), and is naturally such as to increase the intensity of the p-shell symmetries [543] ($L = S = 1$) and [444] ($L = S = 0$) in the lower and upper eigenstates, respectively. For such weak mixing the separation (ΔE) of the two 0^+ states is indeed very sensitive to the p_Λ spin–orbit splitting and varies essentially linearly with ε_p. The ratio (R) of squares of LS density matrix elements, which control the production of the states according to Eq. (3.12), for the upper and lower states is 2.9, to be compared with two in the weak-coupling limit. This ratio increases for $\varepsilon > 0$ ($[f] = [543]$ energetically favored) and decreases as α is made more negative ($S = 0$ favored). Indeed for $\varepsilon = 0.25$ we have $\Delta E = 6.32$, $\beta = 0.11$ and $R = 3.3$ (cf. Bouyssy's calculation [30]).

A comment is in order before R is compared with the experimental ratio of about 3 for the 0° cross sections of the two states. It is that the experimentally measured [43–46] ratio (T) of pickup spectroscopic factors for the $3/2^-$ and $1/2^-$ hole states in ${}^{15}O$ (or ${}^{15}N$) is always less than 2 and perhaps as low as 1.5, substantial fractions of the $p_{3/2}$ pick-up strength missing from the 6.18 MeV level being found [43–44] in

^{15}O states at 9.61 and 10.48 MeV. Thus if p_Λ particles are coupled to the physical ^{15}O core states

$$R^{1/2} = \frac{\{T(1-\beta^2)\}^{1/2} + \beta}{-T^{1/2}\beta + (1-\beta^2)^{1/2}} \tag{5.12}$$

which depends quite strongly on T. Finally there are the dynamical effects on R to be considered. These can be estimated from our full reaction calculation. In addition to the four peaks in the $^{16}O(K^-, \pi^-)\,^{16}_{\Lambda}O$ (0°) spectrum discussed above there is a broad structure centered near $B_\Lambda = -15$ MeV [2]. It can be attributed mainly to the $s_N \to s_\Lambda\, \Delta L = 0$ transition with some $p_N \to (sd)_\Lambda\ \Delta L = 1$ excitation, both of which are expected in this energy region.

The $(p_N^{-1} p_\Lambda)\, 2^+$ states in our standard calculation remain relatively pure weak-coupling states. The state based on the $p_{1/2}$ hole is shifted down from the corresponding 0^+ state by 0.3 MeV. The centroid of the two states, 1 MeV apart, based on the $p_{3/2}$ hole, lies even closer to the corresponding 0^+ state. The ratio for the production of the upper pair relative to the lowest state is 1.8, before any account is taken of the fractionation of the pickup strength to the core. In addition, $\Delta L = 1$ strength, from an s_Λ coupled to the 9.61- and 10.48-MeV states of the core, will contribute to the peak at $B_\Lambda \approx 2.5$ MeV.

5.3.4. *The Hypernucleus* $^{12}_{\Lambda}C$

The $^{12}C(K^-, \pi^-)\,^{12}_{\Lambda}C$ reaction has been studied [2] at CERN for $\theta_\pi = 0°$ and $p_K = 715$ MeV/c and at BNL [6] for $\theta_\pi \leqslant 19°$ and $p_K = 800$ MeV/c. The 0° spectrum exhibits two peaks at $B_\Lambda = 11$ and 0 MeV which have ascribed [2, 6, 20] to 1^- and 0^+ states, respectively, in which a Λ particle in an $s_{1/2}$ or a $p_{3/2}$ orbit couples to the $3/2^-$ ^{11}C ground state, the dominant parent of the ^{12}C ground state. For $\theta_\pi > 0°$ the two peaks remain [6], the upper peak showing no observable shift in excitation energy. The angular distributions [6] are consistent with the excitation of both $(^{11}C(\text{g.s.}) \otimes p_{3/2\Lambda})\, 0^+$ and $(^{11}C(\text{g.s.}) \otimes p_{1/2\Lambda}, p_{3/2\Lambda})\, 2^+$ configurations in the $B_\Lambda =$ 0 MeV peak [6, 20], the $\Delta L = 2$ excitation being totally dominant [20] for $\theta_\pi = 15°$.

In the full $p^7 p_\Lambda$ shell-model calculation the tendency to form states with good spatial symmetry means that the wavefunctions of the low-lying 0^+ and 2^+ states differ considerably from the simple weak-coupling description given above. The end result that the $\Delta L = 0$ and $\Delta L = 2$ strength should be localized at the same excitation energy is, however, the same in both descriptions. Nevertheless it is instructive to examine the shell-model calculation for the 0^+ states in some detail.

The only core states that we need consider are the $3/2^-$ ground state, the 2.00-MeV $1/2^-$ state and the 4.80-MeV $3/2^-$ state. These three states account for essentially all the p-shell pickup strength from ^{12}C, with individual spectroscopic amplitudes [15] of 2.387, 1.227 and 0.869, respectively. The wave functions of these levels have dominantly [43] spatial symmetry (hence $S = 1/2$). Their orbital angular momentum content for [43] symmetry is

$$|3/2_1^-\rangle = 0.783|L=1\rangle - 0.465|L=2\rangle + ...,$$
$$|1/2^-\rangle = 0.974|L=1\rangle + ..., \tag{5.13}$$
$$|3/2_2^-\rangle = 0.451|L=1\rangle + 0.822|L=2\rangle + ...$$

If we now couple a p_Λ to the [43] symmetry we obtain the hypernuclear symmetries [53], [44] and [431] with lowest L values of 1, 0 and 1, respectively (and $S = L$ for $J = 0$). We find the amplitudes of these symmetries in the weak-coupling basis states by first converting the weak-coupling basis states to LS coupling and then using the appropriate $SU3 \supset R3$ Clebsch–Gordan coefficients to obtain the amplitudes of states with definite spatial symmetry. The result of these transformations is given in Table VI. Also given are the 0^+ wave functions of the standard calculation and their decomposition in terms of the states with good spatial symmetry. While the weak-coupling configurations are quite strongly mixed in the 0^+ eigenstates it is clear that one spatial symmetry dominates in each 0^+ wave function. For the standard ΛN interaction the $[44]\, L = 0$ configuration which is strongly populated in the (K^-, π^-) reaction comes lowest. However, for $V_{\Lambda N} \approx V_{NN}$ the $|53]\, L = 1$ configuration will come lowest as shown in Fig. 14. Then the 0_2^+ and 0_3^+ states, which are the analogs

TABLE VI

Wave Function Relationships for $^{12}_{\Lambda}C(0^+)$

A	$\|53]\, L=S=1$	$\|44]\, L=S=0$	$\|431]\, L=S=1$
$3/2_1^- \otimes p_{3/2}$	−0.045	0.639	0.647
$3/2_2^- \otimes p_{3/2}$	−0.730	0.368	−0.460
$1/2^- \otimes p_{1/2}$	0.607	0.562	−0.513

B	$3/2_1^- \otimes p_{3/2}$	$3/2_2^- \otimes p_{3/2}$	$1/2^- \otimes p_{1/2}$
0_1^+	0.886	0.078	0.458
0_2^+	−0.320	−0.611	0.724
0_3^+	0.336	−0.788	−0.516

C	$\|53]\, L=S=1$	$\|44]\, L=S=0$	$\|431]\, L=S=1$
0_1^+	0.181	0.852	0.302
0_2^+	0.900	−0.022	−0.297
0_3^+	0.247	−0.391	0.868

[A] Symmetry content of weak-coupling basis states. Note that only the most important states with definite spatial symmetry are listed.

[B] Expansion of 0^+ eigenstates in the weak-coupling basis. The energies of the three 0^+ states are 0, 2.26 and 5.51 MeV.

[C] Symmetry content of 0^+ eigenstates.

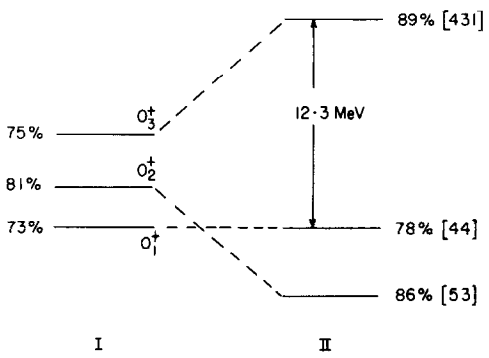

FIG. 14. The three lowest $p^7p_\Lambda\, 0^+$ states of $^{12}_{\Lambda}C$ for the standard ΛN interaction (I) and for $V_{\Lambda N} \approx V_{NN}$ (II). The intensities of the dominant spatial symmetries in the wave functions are also given.

of the 0_1^+, and 0_2^+ states in the nuclear calculation, are separated by 12 MeV or so. The full low-energy spectrum of $p^7p_\Lambda\, 0^+$ and 2^+ states is given in Fig. 15 together with the squares of the density matrix elements governing the production of the states. The bulk of the 2^+ strength is fragmented over the lowest three levels the centroid of this strength coinciding with that of the corresponding 0^+ strength to within 150 keV. This feature of p^7p_Λ strength is preserved for a wide range of parameter variations in the interaction, including strong one-body spin–orbit forces. Consequently little can be deduced about this interaction from the $^{12}C(K^-, \pi^-)\, ^{12}_{\Lambda}C$ data.

In contrast it is probable that the $^{12}C(K^-, \pi^-)\, ^{12}_{\Lambda}C$ reaction can be used to put useful constraints on the nature of the $N\Lambda$ interaction for $p_N s_\Lambda$. The issue is the formation strength of the second and third 1^- levels in $^{12}_{\Lambda}C$ which in the weak-coupling limit would be formed by coupling an s_Λ to the $1/2^-$, 2.00-MeV and $3/2^-$,

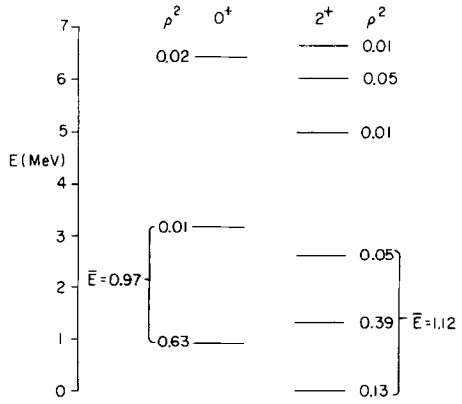

FIG. 15. The spectrum of the lowest $p^7p_\Lambda\, 0^+$ and 2^+ states of $^{12}_{\Lambda}C$ for the standard ΛN interaction. For each level the square of the LS density matrix element appearing in Eq. (3.12) is given. Note the near equality of the centroid energies for the lowest groups of 0^+ and 2^+ levels.

4.80-MeV excited states of ^{11}C. In the weak-coupling limit the summed strength to these two states would be 40% of the ground-state strength, if Cohen and Kurath's spectroscopic factors [15] are used. Many experimental measurements of the pickup strength have been made [45, 47] and overall there is good agreement with the theoretical values [15]. From a study of the $^{12}C(K^-, \pi^-)\,^{12}_{\Lambda}C$ reaction, Chrien *et al.* [6] have found only $6 \pm 5\%$ of the ground-state strength in the 2- to 7-MeV region of excitation energy in $^{12}_{\Lambda}C$. The most natural explanation of this lack of strength lies in destructive admixtures of the weak-coupling basis states in the second and third 1^- levels.

The canonical $p_N s_\Lambda$ interaction ($\Delta^+ S^+ Q^0_{00}$; 79), favored by Dalitz and Gal [17], actually gives an increase of strength for the second and third 1^- levels while $\alpha < 0$, Eq. (3.16), by itself gives a decrease. It is clear that the $^{12}C(K^-, \pi^-)\,^{12}_{\Lambda}C$ data can put useful constraints on the $p_N s_\Lambda$ effective interaction, which cannot be regarded as well determined solely from a fit to ground state binding energies [28]. The strongest constraints on the interaction are expected from hypernuclear γ-ray data on energies of excited states and core $\otimes\, s_\Lambda$ doublet splittings.

5.3.5. *The Hypernucleus* $^{14}_{\Lambda}N$

The $^{14}N(K^-, \pi^-)\,^{14}_{\Lambda}N$ reaction has been studied [7] at *BNL* for $\theta_\pi = 0°$ and $p_K = 800$ MeV/c. The most prominent features in the spectrum are peaks at $E_x = 10.5$ and 20 MeV, which can be associated with two groupings of strength for neutron pickup from ^{14}N.

Five states which can clearly be identified [48] with p-shell configurations have been observed in neutron pickup from ^{14}N. There is good agreement between experiment [45, 49] and theory [15] for the spectroscopic factors. The five states are the $1/2^-$ ground state; the $3/2^-$ 3.51-MeV level, the $5/2^-$, 7.38-MeV level; the $1/2^-$ 8.92-MeV level and the $3/2^-$ 11.88-MeV level with theoretical [15] C^2S values of 0.69, 0.16, 1.86, 0.67 and 1.16, respectively. The ground state is populated by $p_{1/2}$ pickup, the rest mainly by $p_{3/2}$ pickup. The [441] symmetry content of the five core wave functions is 70.6, 87.7, 83.4, 2.4 and 1.9%, the rest being [432] symmetry (very little [333]). The [441] and [432] symmetries are reached by pickup from the dominant (91%) [442] component of the ^{14}N ground state in the ratio of 1:2, $S = 3/2$ states with [432] symmetry being favored over those with $S = 1/2$ in the ratio 4:1. Indeed the $1/2^-_2$ and $3/2^-_2\, p^9$ wave functions contain 89.8 and 71.0% of quartet configurations, respectively.

In a simple weak-coupling picture we expect a $p^9 p_\Lambda\, 1^+$ state based on the ^{13}N ground state to be a major contributor to the 0° cross section of the 10.5-MeV peak and 1^+ states based on the 7.38-, 8.92- and 11.88-MeV levels of ^{13}N to be responsible for the strong excitation of the 20-MeV peak. From Fig. 16 it can be seen that the essential features of the weak-coupling description remain in the shell-model calculation with our standard ΛN interaction. Indeed, the two strongest 1^+ states contain 87% ($5/2^-_1 \otimes p_{3/2\Lambda}$) and 81% ($3/2^-_2 \otimes p_{3/2\Lambda}$), respectively. Figure 17a shows that the $\Delta L = 0$ strength in the $E_x \approx 10$-MeV region is augmented by $p_N \to s_\Lambda\, \Delta L = 1$ strength; the $\Delta L = 1$ strength at lower excitation energies does not show up clearly in

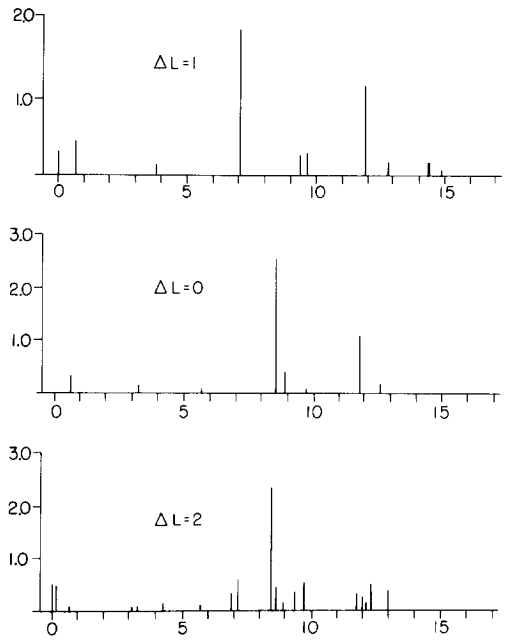

FIG. 16. Formation strengths for ${}^{14}_{\Lambda}N$ states. See caption to Fig. 10.

the forward angle data (Fig. 17b). There is a tendency for the lowest p^9p_Λ configurations to develop [541] symmetry and 38% of the $\Delta L = 0$ strength associated with the two lowest core states is shifted into the 20-MeV peak. The relationship between the weak-coupling wave functions and wave functions with good spatial symmetry is easily found. For example, since the ${}^{14}N$ ground state is 90% [442] $L = 2$ $S = 1$ we require, in analogy to Eqs. (5.6) and (5.11),

$$|[441] \otimes [1] \rightarrow [442]\, L = 2\rangle = -\sqrt{21/25}\,|L_c = 3 \otimes p_\Lambda\rangle - \sqrt{4/25}\,|L_c = 1 \otimes p_\Lambda\rangle,$$
$$|[432] \otimes [1] \rightarrow [442]\, L = 2\rangle = \sqrt{3/4}\,|L_c = 2 \otimes p_\Lambda\rangle - \sqrt{1/4}\,|L_c = 1 \otimes p_\Lambda\rangle. \quad (5.14)$$

Thus the first configuration coupled to $S = 1$ to form $J = 1$ has an overlap of 84% with $|[441]\, L_c = 3 S_c = 1/2;\ J_c = 5/2 \otimes p_{3/2\Lambda}\rangle$ which in turn has a large overlap (83%) with the $|5/2^-_1 \otimes p_{3/2\Lambda}\rangle$ weak-coupling state. The distribution of $\Delta L = 2$ strength (Fig. 16 and Fig. 17b) is quite similar to the $\Delta L = 0$ strength. By far the strongest state is a 3^+ state based almost entirely (99%) on the $5/2^-$ core state

$$|3^+\rangle = 0.930\,|5/2^- \otimes p_{1/2\Lambda}\rangle + 0.350\,|5/2^- \otimes p_{3/2\Lambda}\rangle + \ldots. \quad (5.15)$$

Finally we note that the experimental and theoretical forward angle cross sections shown in Fig. 17 are in good agreement. The experimental cross sections [50] for the 10.5- and 20-MeV peaks, after the subtraction of K decay and quasi-free backgrounds, are 458 ± 56 and 1785 ± 104 μb/sr, respectively. The theoretical cross

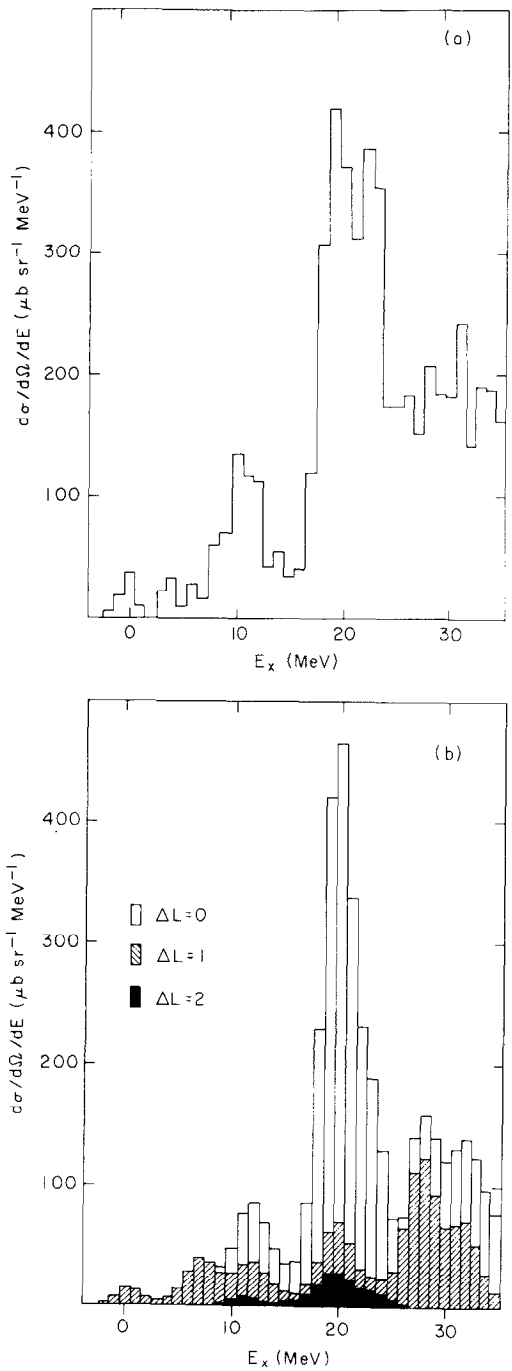

FIG. 17. Direct comparison between the $^{14}N(K^-,\pi^-)\,^{14}_{\Lambda}N$ data and theory for a laboratory angle of 4°. The theoretical cross sections were smeared with a Gaussian of width 3.5 MeV.

sections taken over the same regions of excitation energy are 434 and 2028 μb/sr. Some of the subtracted quasi-free background at the highest excitation energies can be accounted for by $s_N \to s_\Lambda$ and $p_N \to (sd)_\Lambda$ transitions for which the strength is estimated in Fig. 17b. The only obvious discrepancy between theory and experiment in Fig. 17 appears to be a difference of about an MeV in the separation of the two clearly observable peaks.

5.3.6. *The Hypernucleus* $^{14}_{\Lambda}C$

The neutron pickup strength from ^{14}C is concentrated [15] in three levels of ^{13}C, the $1/2^-$ ground state, the 3.68-MeV $3/2^-$ level and the 15.11-MeV $3/2^-$, $T = 3/2$ level with C^2S values of 1.73, 2.04 and 1.19, respectively. In many respects the spectra for the $^{14}C(K^-, \pi^-)\,^{14}_{\Lambda}C$ reaction are expected to be similar to spectra taken with a ^{13}C target. It can be seen from Fig. 18 that the ratio of $\Delta L = 0$ strength for the two lowest 0^+ states is changed from 1.2 in the weak-coupling limit to 4.0 in the standard calculation; the lower state tends toward [541] symmetry with $L = S = 1$ and the upper state to [442] symmetry with $L = S = 0$. As in $^{13}_{\Lambda}C$, a shift in the $\Delta L = 2$ strength relative to the $\Delta L = 0$ strength based on the $3/2^-_1$ core state is expected, although it is possible that this shift could be obscured by $\Delta L = 1$ strength based on the lowest $T = 3/2$ core state.

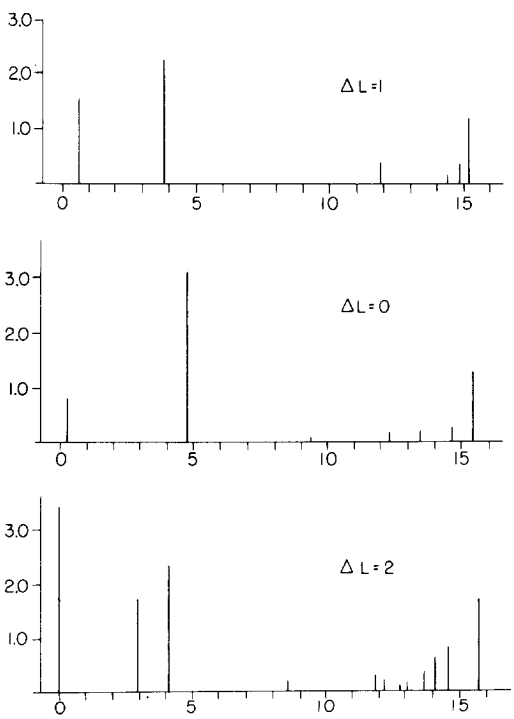

FIG. 18. Formation strengths for $^{14}_{\Lambda}C$ states. See caption to Fig. 10.

5.3.7. *The Hypernucleus* $^{15}_{\Lambda}N$

Substantial strength for neutron pickup from ^{15}N is observed [51] for seven levels of ^{14}N: the 1^+; $T=0$ ground state, the 0^+; $T=1$, 2.31-MeV level, the 1^+; $T=0$, 3.95-MeV level, the 2^+; $T=0$ 7.03-MeV level, the 2^+; $T=1$ 9.17-MeV level; the 2^+; $T=1$ 10.43-MeV level and the 1^+; $T=1$ 13.71-MeV level. There is good agreement between theory [15] and experiment if the well known mixing [51, 52] between the lowest p^{10} 2^+; $T=1$ configuration and a $p^8(sd)^2$ configuration is taken into account (9.17- and 10.43-MeV levels). The wide spread in pickup strength leads to the broad distribution of hypernuclear formation strength shown in Fig. 19 for $\Delta L=0, 1, 2$. With the current energy resolution of about 2.5 MeV it is doubtful whether peaks corresponding to states displayed in Fig. 19 could be resolved. Thus, at the present time, $^{15}_{\Lambda}N$ does not appear to be an attractive case for experimental study.

5.3.8. *The Hypernucleus* $^{10}_{\Lambda}B$

Neutron pickup strength is observed to five states in ^9B: the $3/2^-$ ground state, the $5/2^-$ 2.36-MeV level, the $7/2^-$ 6.97-MeV level, the $(7/2^-)$ 11.7-MeV level and the $(5/2^-)$ 14.7-MeV level with theoretical C^2S values of 0.59, 0.58, 0.56, 0.78 and 0.24. Here we have used Cohen and Kurath's (6–16) 2BME interaction [15] which appears to give a better description of the $A=9$ data than the POT interaction. Even so the $7/2^-$ and $5/2^-$ levels which we identify with the 11.7- and 14.7-MeV levels are

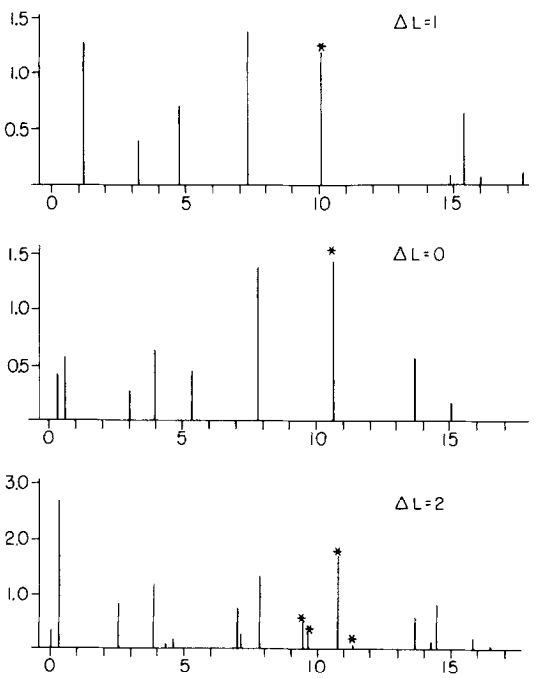

FIG. 19. Formation strengths for $^{15}_{\Lambda}N$ states; see caption to Fig. 10. Asterisks indicate 2^+; $T=1$ parentage, which in reality will be fragmented over several core states.

predicted ~1.5 MeV too low in energy. It is not clear, then, how realistic the other theoretical energies that we use for the hypernuclear shell-model calculations are. The distribution of formation strength for ${}^{10}_{\Lambda}B$ is given in Fig. 20. The distribution of $\Delta L = 0$ strength differs markedly from that of the pickup strength, of which the distribution of $\Delta L = 1$ strength is representative. It is easy to show that the wave function of the 3^+_3 state

$$0.368|3/2^-_1 \otimes p_{3/2\Lambda}\rangle + 0.632|5/2^-_1 \otimes p_{1/2\Lambda}\rangle - 0.664|5/2^-_1 \otimes p_{3/2\Lambda}\rangle + \ldots \quad (5.16)$$

has a large overlap with the $|[41] \otimes [1] \rightarrow [42]\ K = 2\ L = 2\ S = 1\rangle$ configuration based on the dominant [41] symmetry of the $3/2^-_1$ and $5/2^-_1$ core states. The $\Delta L = 0$ strength at higher excitation energy is due mainly to the $|[32] \otimes [1] \rightarrow [42]\ K = 2\ L = 2\ S = 1\rangle$ configuration. Both [42] configurations have a strong overlap with the ${}^{10}B$ ground-state wave function

$$|{}^{10}B \text{ g.s.}\rangle = 0.871\,|[42]\ K = 2\ L = 2\ S = 1\rangle - 0.401\,|[42]\ K = 2\ L = 3\ S = 1\rangle + \ldots. \quad (5.17)$$

We have again a clear demonstration of the role played by symmetries in the structure of light hypernuclei.

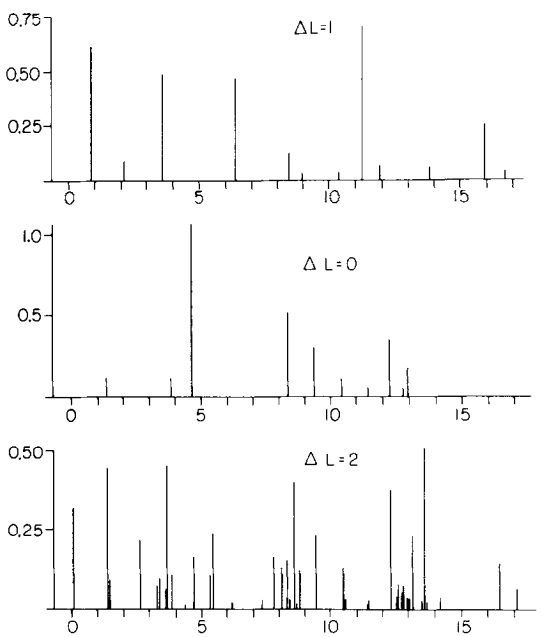

FIG. 20. Formation strengths for ${}^{10}_{\Lambda}B$ states. See caption to Fig. 10.

5.3.9. *The Hypernucleus* ${}^{11}_{\Lambda}B$

In the case of ${}^{11}_{\Lambda}B$ the ${}^{10}B$ core nucleus possesses a relatively high density of states at low excitation energy, all of which are populated [53, 54] in neutron pickup reactions. A consequence of this is a high density of hypernuclear levels (Fig. 21), most with some formation strength, which clearly cannot be resolved experimentally. Also there is strong mixing of the weak-coupling basis states, e.g., the wave function of the $3/2_2^-$ level, with strong $\Delta L = 0$ formation strength is

$$|3/2_2^-\rangle = 0.598\,|3_1^+ \otimes p_{3/2\Lambda}\rangle - 0.625\,|1_1^+ \otimes p_{1/2\Lambda}\rangle + 0.334\,|1_1^+ \otimes p_{3/2\Lambda}\rangle + 0.112\,|1_2^+ \otimes p_{1/2\Lambda}\rangle - 0.192\,|1_2^+ \otimes p_{3/2\Lambda}\rangle + 0.226\,|2_1^+ \otimes p_{1/2\Lambda}\rangle - 0.187\,|2_1^+ \otimes p_{3/2\Lambda}\rangle. \tag{5.18}$$

One possibility, of some interest, is that with the $\Delta L = 1$ strength concentrated at low excitation energy a rather pure $\Delta L = 2$ excitation at $E_x \sim 12$ MeV is possible for $\theta_\pi \sim 15°$.

5.4. $s_N \to s_\Lambda$ *and* $p_N \to (sd)_\Lambda$ *Transitions*

In the preceding sections we have discussed in detail the results of our $p^n p_\Lambda$ shell-model calculations and used the wave functions to estimate $p_N \to p_\Lambda$ cross sections for the (K^-, π^-) reaction. For $p_N \to s_\Lambda$ transitions we have used the results of Gal, Soper

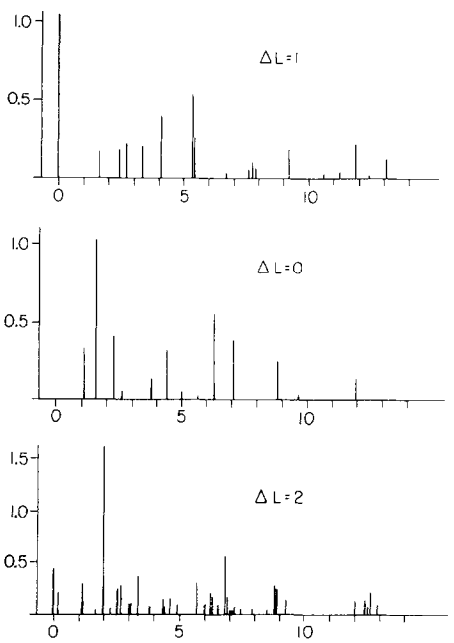

FIG. 21. Formation strengths for ${}^{11}_{\Lambda}B$ states. See caption to Fig. 10.

and Dalitz [28]. Starting at about 20-MeV excitation energy in the residual hypernucleus we expect $s_N \to s_\Lambda$ and $p_N \to (sd)_\Lambda$ transitions to contribute to the (K^-, π^-) cross section. Angular distributions for these transitions are shown in Fig. 8. Estimates of the cross sections for such transitions appear in Figs. 11 and 17 for ${}^{13}_{\Lambda}C$ and ${}^{14}_{\Lambda}N$, respectively. We discuss briefly how these estimates were made.

First we note that the single-particle wave functions which enter into the distorted-wave reduced amplitudes β^k_m of Eq. (2.6) are functions of the relative coordinate between the particle and the core. The conventional shell-model spectroscopic factor corresponds to splitting off a single-particle wave function which is a function of the particle coordinate with respect to the origin of the potential well. To obtain the appropriate function in terms of the relative coordinate the shell-model spectroscopic amplitude must be multiplied, in an oscillator model, by $(A/A-1)^{Q/2}$, where $Q = 2n + l$ gives the node structure of the single-particle wave function. Then for a p-shell target nucleus the sum rule for pickup of a p nucleon is $(A/A-1)(A-4)$. The sum rule for s- nucleons is correspondingly less than four after spurious center of mass components are eliminated from the s-hole states, and is, in fact, equal to $3(A/A-1)$. The distribution of s-hole strength, as located in $(p, 2p)$ reactions [55], is very broad. Our estimates for the strength associated with $s_N \to s_\Lambda$ transitions are based on concentrating the sum-rule strength in a single peak with a location and a width based on the $(p, 2p)$ spectra of Tyren *et al.* [55]. For a ${}^{14}N$ target, e.g., the neutron pickup sum rule is 21/13 and we have concentrated the calculated 4° (K^-, π^-) cross section of 767 μb/sr (Eq. (3.15) and Fig. 8) at an excitation energy of 33 MeV with a width of 10 MeV. If $(p, 2p)$ results are not available the distribution of s-hole strength from shell-model calculations [56] can be used. A study of neutron-hole states in the s- shell has been made [4] using the (K^-, π^-) reaction on ${}^6Li$, ${}^7Li$, ${}^9Be$ and ${}^{12}C$ targets. The $s_N \to s_\Lambda$ transitions show up very clearly for the Li targets.

In the case of $p_N \to (sd)_\Lambda$ transitions we ignore center of mass corrections and use Eq. (3.15) directly, assuming pure weak coupling and a 10-MeV spacing between the p_Λ and $(sd)_\Lambda$ orbits.

Despite the fact that the above estimates for $s_N \to s_\Lambda$ and $p_N \to (sd)_\Lambda$ transition strength are somewhat crude, particularly for the $p_N \to (sd)_\Lambda$ strength, it appears that much of the observed hypernucleus production at high excitation energies can be accounted for; see, e.g., Figs. 11 and 17.

6. Conclusions

In this paper we have developed a comprehensive approach to hypernuclear spectroscopy in the p shell. The (K^-, π^-) reaction mechanism is treated in DWBA, and incorporates realistic K^- and π^- distorted waves obtained from an optical model fit to the available elastic scattering data, Fermi-averaged $K^- n \to \pi^- \Lambda$ amplitudes, and $\{n, \Lambda\}$ bound-state wave functions constrained by empirical binding energies and, in some cases, rms radii. A weak-coupling *basis* is used to describe the hypernuclear structure aspects. Since the intensities of hypernuclear states (summed over the spin)

seen in the (K^-, π^-) reaction are proportional to the neutron pickup strengths on the same target (in the weak-coupling limit), enough nuclear core states are included to account for essentially all of the pickup strength. In some cases the mixing of configurations based on different core states has a significant effect on hypernuclear formation strengths.

The existing (K^-, π^-) data on ${}^{9}_{\Lambda}Be$, ${}^{12}_{\Lambda}C$, ${}^{13}_{\Lambda}C$, ${}^{14}_{\Lambda}N$ and ${}^{16}_{\Lambda}O$ are analyzed in detail, and used to extract constraints on $V_{\Lambda N}$ and obtain spin assignments for hypernuclear levels. In agreement with earlier work, we find that weak spin–spin, space-exchange and spin–orbit interactions for ΛN are consistent with the data. The measured energy shifts of peaks in the (K^-, π^-) spectra as the pion angle is varied are used to obtain constraints on the spin–orbit splitting ($\varepsilon_p \approx 0.5$ MeV) and the quadrupole part of the ΛN interaction ($3.0 < -F_2 < 3.4$ MeV). Even though the ΛN interaction is fairly weak (compared to NN, say), hypernuclei display a tendency to seek a high degree of spatial symmetry (forbidden for systems with only nucleons) in certain low-lying states. This configuration-mixing effect can lead to approximate dynamical selection rules ([441] $\not\to$ [54] for $\Delta L = 0$ transitions in ${}^{13}_{\Lambda}C$, for instance) and considerable deviations in intensity ratios from the weak-coupling limit in some cases. In addition to explaining observed intensity ratios of lines seen in the (K^-, π^-) reaction on a variety of targets, our approach provides a qualitative account of absolute cross sections (at the 20% level) and the shapes of (K^-, π^-) angular distributions.

We have also given predictions for several p-shell hypernuclei for which no data exist, namely, ${}^{10}_{\Lambda}B$, ${}^{11}_{\Lambda}B$, ${}^{14}_{\Lambda}C$ and ${}^{15}_{\Lambda}N$. Except for ${}^{14}_{\Lambda}C$, the spectra are rather complicated, involving a variety of states which are not too well separated in energy. Using coarse resolution (K^-, π^-) experiments, it will be difficult to make much further progress in extracting the detailed spin dependence of the ΛN interaction. Energy resolution of the order of 100–200 keV in (K^-, π^-) is required before one can expect further qualitative advances in hypernuclear spectroscopy in the p shell. This certainly demands the intense K^- beams of a "kaon factory." Even in this case, the unnatural parity part of the Λ hypernuclear spectrum would remain essentially unexplored. For this part of the spectrum, the $(K^-, \pi^-\gamma)$ [17, 57] and (γ, K^+) reactions [58] offer particular promise. The existence of more detailed hypernuclear data, particularly regarding spin splittings of levels, would warrant a serious attempt to relate the sort of phenomenological ΛN potentials used here to more microscopic descriptions such as meson or quark–gluon exchange models; even now, there is a challenge for microscopic theories to explain the overall strength and general characteristics of the empirical $N\Lambda$ effective interaction. The $(K^-, \pi^-\gamma)$ data taken so far [57] imply small doublet splittings for $p^n s_\Lambda$ configurations and hence a small $\mathbf{l}_{N\Lambda} \cdot \mathbf{s}_\Lambda$ interaction consistent with the analysis of $p_N \to p_\Lambda$ transitions in the (K^-, π^-) reaction.

The shell-model calculations described in this paper may be extended in various ways. For example, all $1\hbar\omega$ hypernuclear configurations can be treated on the same footing if the data warrants; such a treatment is necessary in any case for the lightest p-shell hypernuclei to deal with center of mass problems and to treat properly the excitation of levels via $s_N \to s_\Lambda$ transitions [59]. Also, we have made calculations for

Σ hypernuclei using a $p^n p_\Sigma$ shell-model basis under the assumption that isospin is a good quantum number. More parameters are needed to specify the $N\Sigma$ effective interaction since two isospins are possible for the two-body system; baryon–baryon potentials [33] suggest a strong spin and isospin dependence for the $N\Sigma$ interaction and a larger one-body spin–orbit Σ-nucleus interaction [32] than in the case of the Λ. Additional complications are that isospin is likely not to be a good quantum number for some Σ-hypernuclear levels and that continuum effects may be important. As more data becomes available on Λ, Σ, Ξ and possibly even Ω^- hypernuclei in the future, a more detailed study of spectroscopic questions along the general lines developed here will be warranted.

REFERENCES

1. G. C. BONAZZOLA *et al.*, *Phys. Rev. Lett.* **34** (1975), 683; W. BRÜCKNER *et al.*, *Phys. Lett. B* **55** (1975), 107; **62** (1976), 481.
2. W. BRÜCKNER *et al.*, *Phys. Lett. B* **79** (1978), 157; R. BERTINI *et al.*, *Phys. Lett. B* **90** (1980), 375.
3. R. BERTINI *et al.*, *Nucl. Phys. A* **360** (1981), 315.
4. R. BERTINI *et al.*, *Nucl. Phys. A* **368** (1981), 365.
5. B. POHV, *in* "Annual Review of Nuclear and Particle Science" (J. D. Jackson, H. E. Gove, and R. F. Schwitters, Eds.), Vol. 28, p. 1, Annual Reviews, Inc., Palo Alto, 1978; B. POHV, *Nucl. Phys. A* **335** (1980), 233. These articles review the CERN work on (K^-, π^-) reactions.
6. R. CHRIEN *et al.*, *Phys. Lett. B* **89** (1979), 31.
7. M. MAY *et al.*, *Phys. Rev. Lett.* **47** (1981), 1106.
8. D. H. DAVIS AND J. SACTON, *in* "High Energy Physics" (E. H. S. Burhop, Ed.), Vol. II, pp. 365–455, Academic Press, New York, 1967; J. PNIEWSKI AND D. ZIEMINSKA, "Proceedings, Seminar on Kaon-Nuclear Interaction and Hypernuclei, Zvenigorod, USSR, September 1977," pp. 33–50.
9. E. H. AUERBACH *et al.*, *Phys. Rev. Lett.* **47** (1981), 1110.
10. J. HÜFNER, S. Y. LEE, AND H. A. WEIDENMÜLLER, *Phys. Lett. B* **49** (1974), 409; *Nucl. Phys. A* **234** (1974), 429; H. C. CHIANG AND J. HÜFNER, *Phys. Lett. B* **84** (1979), 393.
11. A. BOUYSSY, *Nucl. Phys. A* **290** (1977), 324.
12. D. MARLOW *et al.*, *Phys. Rev. C* **25** (1982), 2619; D. MARLOW, Thesis, Carnegie Mellon University, 1981.
13. P. D. KUNZ, unpublished. The coupled channels code CHUCK was utilized with no back coupling, a mode in which its results are exactly equivalent to DWBA.
14. G. P. GOPAL *et al.*, *Nucl. Phys. B* **119** (1977), 362.
15. S. COHEN AND D. KURATH, *Nucl. Phys.* **73** (1965), 1; *Nucl. Phys. A* **101** (1967), 1.
16. D. J. MILLENER, unpublished.
17. R. H. DALITZ AND A. GAL, *Ann. Phys. (N.Y.)* **116** (1978), 167.
18. M. L. GOLDBERGER AND K. M. WATSON, "Collision Theory," p. 94, Wiley, New York, 1964.
19. D. M. BRINK AND G. R. SATCHLER, "Angular Momentum," Oxford Univ. Press (Clarendon), Oxford, 1968.
20. C. B. DOVER, A. GAL, G. E. WALKER, AND R. H. DALITZ, *Phys. Lett. B* 98 (1979), 26.
21. L. LUDEKING, Ph.D. thesis, unpublished, 1979; C. B. DOVER, L. LUDEKING, AND G. E. WALKER, *Phys. Rev. C* **22** (1980), 2073.
22. N. AUSTERN, "Direct Nuclear Reaction Theories," Wiley, New York, 1970.
23. E. H. AUERBACH, *Comp. Phys. Comm.* **15** (1978), 165.
24. We use the amplitudes in Table 4e from Ref. [14].
25. B. R. MARTIN AND M. K. PIDCOCK, *Nucl. Phys. B* **127** (1977), 266, 285.

26. E. S. MILLER, Princeton Report PPAD 630F, 1967, unpublished.
27. B. W. ALLARDYCE *et al.*, *Nucl. Phys. A* **209** (1973), 1.
28. A. GAL, J. M. SOPER, AND R. H. DALITZ, *Ann. Phys. (N.Y.)* **63** (1971), 53; **72** (1972), 445; **113** (1978), 79.
29. R. H. DALITZ AND A. GAL, *Phys. Rev. Lett.* **36** (1976), 362; *Ann. Phys. (N.Y.)* **131** (1981), 314.
30. A. BOUYSSY, "Proceedings, International Conference on Nuclear Physics, Berkeley 1980," LBL-11118, p. 146.
31. R. H. DALITZ, R. C. HERNDON, AND Y. C. TANG, *Nucl. Phys. B* **47** (1972), 109.
32. C. B. DOVER AND A. GAL, Brookhaven Report BNL 30124, *in* "Progress in Particle and Nuclear Physics" (D. H. Wilkinson, Ed.), in press.
33. M. M. NAGELS, T. A. RIJKEN, AND J. J. DESWART, *Phys. Rev. D* **12** (1975), 744; *D* **15** (1977), 2547; *D* **20** (1979), 1633.
34. J. V. NOBLE, *Phys. Lett. B* **89** (1980), 325; A. BOUYSSY, *Phys. Lett. B* **99** (1981), 305; R. BROCKMANN AND W. WEISE, *Nucl. Phys. A* **355** (1981), 365.
35. A. BOUYSSY, *Phys. Lett. B* **91** (1980), 15.
36. A. H. WAPSTRA AND K. BOS, *Atomic Nucl. Data Tables* **19** (1977), 177.
37. M. JURIC *et al.*, *Nucl. Phys. B* **52** (1973), 1.
38. T. CANTWELL *et al.*, *Nucl. Phys. A* **236** (1974), 445.
39. H. TAKETANI, J. MUTO, H. YAMAGUCHI, AND J. KOKAME, *Phys. Lett. B* **27** (1968), 625; J. D. COSSAIRT AND D. P. MAY, *Nucl. Phys. A* **319** (1979), 182.
40. F. AJZENBERG-SELOVE, *Nucl. Phys. A* **320** (1979), 1.
41. H. D. KNOX AND R. O. LANE, *Nucl. Phys. A* **359** (1981), 131.
42. H. BANDO, M. SEKI, AND Y. SHONO, *Prog. Theor. Phys.* **66** (1981), 2118.
43. J. SNELGROVE AND E. KASHY, *Phys. Rev.* **187** (1969), 1246.
44. G. MAIRLE AND G. J. WAGNER, *Z. Phys.* **258** (1973), 321; V. BECHTOLD, L. FRIEDRICH, P. DOLL, K. T. KNÖPFLE, G. MAIRLE, AND G. J. WAGNER, *Phys. Lett. B* **72** (1977), 169.
45. P. G. ROOS, S. M. SMITH, V. K. C. CHENG, G. TIBELL, A. A. COWLEY, AND R. A. J. RIDDLE, *Nucl. Phys. A* **255** (1975), 187.
46. M. A. FIRESTONE, J. JÄNECKE, A. DUDEK-ELLIS, P. J. ELLIS, AND T. ENGELAND, *Nucl. Phys. A* **258** (1976), 317; J. D. COSSAIRT, S. B. TALLEY, D. P. MAY, R. E. TRIBBLE, AND R. L. SPROSS, *Phys. Rev. C* **18** (1978), 23.
47. F. AJZENBERG-SELOVE AND C. L. BUSCH, *Nucl. Phys. A* **336** (1980), 1.
48. D. G. FLEMING, J. CERNY, C. C. MAPLES, AND N. K. GLENDENNING, *Phys. Rev.* **166** (1968), 1012 and references contained therein.
49. F. HINTERBERGER, G. MAIRLE, V. SCHMIDT-ROHR, P. TUREK, AND G. J. WAGNER, *Nucl. Phys. A* **106** (1968), 161.
50. S. BART *et al.*, private communication.
51. J. SNELGROVE AND E. KASHY, *Phys. Rev.* **187** (1969), 1259; W. BOHNE, H. HOMEYER, H. LETTAU, H. MORGENSTERN, J. SCHEER, AND F. SICHELSCHMIDT, *Nucl. Phys. A* **154** (1970), 105.
52. S. LIE, *Nucl. Phys. A* **181** (1972), 517; G. KASCHL *et al.*, *Nucl. Phys. A* **178** (1971), 275; D. G. FLEMING *et al.*, *Nucl. Phys. A* **162** (1971), 225.
53. L. A. KULL AND E. KASHY, *Phys. Rev.* **167** (1968), 963; I. S. TOWNER, *Nucl. Phys. A* **126** (1969), 97.
54. D. DEHNHARD, N. WILLIAMS, AND J. L. YNTEMA, *Phys. Rev.* **180** (1967), 967; *Phys. Rev. C* **1** (1970), 336.
55. H. TYREN *et al.*, *Nucl. Phys.* **79** (1966), 321.
56. M. KIRCHBACH AND H.-U. JÄGER, *Sov. J. Nucl. Phys.* **29** (1979), 614.
57. M. MAY *et al.*, to be published.
58. A. M. BERNSTEIN, T. W. DONNELLY, AND G. EPSTEIN, *Nucl. Phys. A* **358** (1981), 195c.
59. L. MAJLING *et al.*, *Phys. Lett. B* **92** (1980), 256; L. MAJLING *et al.*, preprint.